Journal of Inflammation Research

Dovepress
Taylor & Francis Group

Open Access Full Text Article

ORIGINAL RESEARCH

Network Pharmacology Combined with Animal Experiments Elucidates the Mechanism of Effect of Xin'an Formula in Treating Allergic Rhinitis

Ming Zhang[1], Ruohui Song[2]

[1]Department of Otorhinolaryngology, The First School of Clinical of Anhui University of Chinese Medicine, Hefei, Anhui, 230012, People's Republic of China; [2]Department of Otorhinolaryngology, The First Affiliated Hospital of Anhui University of CM, Hefei, Anhui, 230031, People's Republic of China

Correspondence: Ruohui Song, Department of Otorhinolaryngology, The First Affiliated Hospital of Anhui University of CM, 117 Meishan Road, Shushan District, Hefei, Anhui, 62850080, People's Republic of China, Email qming659@126.com

Purpose: Exploring the mechanism of the effect of Xin'an BiYan Formula (XBY) in treating allergic rhinitis (AR) using network pharmacology combined with animal experiments.

Methods: Key targets for AR treatment were identified through multi-database and PPI network screening. Potential signaling pathways were predicted by conducting Gene Ontology (GO) and Kyoto Encyclopedia of Genes and Genomes (KEGG) enrichment analyses. The predicted targets and pathways in animal experiments to learn XBY's effects on inflammation and apoptosis in nasal mucosal tissue cells during AR development.

Results: Screening identified 18 principal targets of XBY in AR: TNF, AKT1, HIF1A, MMP9, BCL2, EGFR, IL-2, PTGS2, VCAM-1, PTGS1, ACE, PPARG, ICAM-1, SIRT1, ITGB1, JAK2, RELA, and KIT. The key pharmacological constituents included Genkwanin, Calycosin, Kaempferol, and Luteolin. GO and KEGG enrichment analyses revealed significant enrichment in the PI3K/AKT, Apoptosis, and NF-kappa B signaling pathways. After XBY treatment, infiltration of eosinophils (EOS) and mast cells (MC) in the nasal mucosa of AR model mice was reduced. Concurrently, serum levels of IL-6, TNF-α, COX-2, Total-IgE, OVA-IgE, ICAM-1, and VCAM-1 were decreased. Mucosal levels of p-PI3K/PI3K, p-AKT/AKT, p-n-p65/c-p65, p-IKKβ/ IKKβ, and Bcl-2 proteins were decreased, while Bax, Cleaved-Caspase3, and Caspase-3 protein expression were increased. Cellular levels of reactive oxygen species(ROS) and apoptosis levels were reduced.

Conclusion: The experimental results indicate that the therapeutic effect of XBY on AR is likely mediated through modulation of the ROS/PI3K/AKT/NFκB signaling pathway. By reducing inflammatory cell infiltration, downregulating the expression of inflammatory and adhesion factors, and modulating apoptosis proteins to accelerate inflammatory cell apoptosis, dual mechanisms effectively inhibit the progression of inflammation. This study holds potential translational prospects and may provide new insights for the treatment of AR with TCM.

Keywords: network pharmacology, allergic rhinitis, traditional Chinese medicine, PI3K/AKT signaling pathway, inflammation

Introduction

AR is a pervasive immune-mediated condition and poses a considerable public health issue worldwide. Common clinical manifestations include nasal pruritus, nasal obstruction, rhinorrhea, and episodic sneezing, frequently associated with bronchial asthma, which is marked by recurrent episodes and extended durations.[1] Research epidemiological studies reveal that the worldwide percentage of AR varies between 10% and 40%, substantially impacting patients' daily lives and imposing substantial burdens on healthcare expenditures and socioeconomic factors.[2,3] Currently, first-line pharmacological treatments comprise olfactory steroids, the subsequent generations of oral and nasal antihistamines, and oral leukotriene receptor antagonists, which effectively alleviate symptoms of AR. Nevertheless, continual usage of these medications could result in unfavorable repercussions, including rhinorrhea and heightened drug resistance.[4] Moreover, specific immunotherapy (such as desensitization) and targeted biologics (including anti-IgE monoclonal antibodies)

Received: 1 July 2025
Accepted: 29 October 2025
Published: 3 November 2025

effectively address the underlying cause of the disease; however, they require extended treatment durations and carry an increased risk of adverse effects, which can lead to reduced patient compliance.[5–7] Consequently, the management of AR continues to encounter obstacles, and its pathophysiology and basic treatment approaches are still being explored. Traditional Chinese medicine (TCM), grounded in holism and differential diagnosis and treatment, offers novel clinical alternatives for the prevention and management of AR.

AR is characterized as an immunoglobulin E (IgE)-mediated type I hypersensitivity reaction,[1,8] exhibiting a complex pathogenesis involving multiple inflammatory cells and mediators. Key cellular participants include MC and EOS, while principal inflammatory mediators comprise histamine, IL-6, TNF-α, and PDGF2.[9] The release of these mediators leads to pathological changes, including vasodilation of nasal mucosal vessels and heightened glandular secretion. Simultaneously, it can trigger abnormal expression of adhesion molecules, such as VCAM-1 and ICAM-1, in vascular endothelial and epithelial cells, thereby intensifying the inflammatory response and promoting airway hyperresponsiveness.[10] Previous studies indicate that the PI3K/AKT signaling pathway may have a role in the occurrence of AR by activating MC-mediated allergic responses, intensifying airway hyperresponsiveness, and fostering inflammatory cell infiltration.[11,12] NFκB factors are activated through AKT phosphorylation, consequently facilitating the prolonged release of inflammation-associated mediators that include IL-6, TNF-α, and COX-2.[13] Additionally, oxidative stress caused by increased amounts of ROS constitutes a significant pathogenic mechanism of AR.[14] ROS may trigger the PI3K/AKT signaling pathway, promoting apoptosis in nasal mucosal tissues during the pathogenesis of AR, which exacerbates mucosal barrier impairment and inflammatory responses.[15,16]

TCM exhibits significant effectiveness in treating AR, characterized by enduring outcomes and minimal side effects.[17,18] Clinical investigations demonstrate that the symptomatic remission rate of AR with TCM compound treatment reaches 97.09%. In contrast, the long-term recurrence rate is as low as 24.46%, markedly lower than that of contemporary therapies.[19] Xin'an Zheng's Laryngology is a family practice specializing in laryngological disorders, a lineage that has persisted for 300 years, distinguished by its treatment of nasal congestion (modern medicine refers to it as AR). The XBY is an important formulation utilized by the Laryngology Department of Zheng's Xin'an Medicine for the treatment of AR. It comprises *Ephedra herba* (Ma Huang), *Hedysarum multijugum maxim* (Huang Qi), *Saposhnikoviae radix* (Fang Feng), *Notopterygii rhizome et radix* (Qang Huo), *Radix Paeoniae rubra* (Chi Shao), *Cortex moutan* (Dan Pi), *Tribulifructus* (Ji Li), *radix Rehmanniae* (Sheng Di Huang), *Bombyx batryticatus* (Jiang Can), *Crassostrea gigas* (Mu Li), and *Atractylodes macrocephala koidz* (Bai Zhu). This formula helps reinforce healthy qi to strengthen the body, as well as the lung qi, spleen qi, and kidney qi. It utilizes herbs that clear heat and circulate blood, focusing on the treatment of stasis-heat. Clinical observations have shown that XBY exhibits therapeutic effects; however, the mechanism by which this formula treats AR remains unclear. This study aims to elucidate the probable mechanism of XBY intervention in AR by a combination of network pharmacology and animal experiments. Network pharmacology will integrate the pharmacodynamic mechanisms of XBY, visually presenting the target mechanisms for treating AR and explaining the rationale behind the herbal formula's composition. Subsequently, animal experiments will demonstrate the predicted mechanism pathways, providing a sound theoretical basis for XBY's treatment of AR. This research aims to provide a new perspective on the clinical diagnosis and treatment of AR.

Materials and Methods

Network Pharmacology Analysis of Prospective Targets for the XBY in Treating AR

Procurement of Pharmacologically Active Compounds and Their Respective Targets

The subsequent entries were incorporated into the TCMSP Chinese herbal medicine database (https://old.tcmsp-e.com/tcmsp.php/) and the HERB Chinese herbal medicine database (http://herb.ac.cn/): *Ephedra herba, Hedysarum multijugum maxim, Saposhnikoviae radix, Notopterygii rhizome et radix, radix Paeoniae rubra, Cortex moutan, Tribulifructus, radix Rehmanniae, Bombyx batryticatus, Crassostrea gigas*, and *Atractylodes macrocephala koidz*. The criteria used to assess effective components included having an oral bioavailability (OB) of 30% or more, drug-like properties (DL) of 0.18 or higher, and meeting Lipinski's five rules for drug-like features (molecular weight ≤ 500, H-bond acceptors ≤ 10, H-bond donors ≤ 5, and MlogP ≤ 5). SMILES numbers were acquired from PubChem (https://pubchem.ncbi.nlm.nih.gov/) and transferred to the SwissADME database (http://

www.swissadme.ch/). Subsequent evaluation for efficacious components was conducted utilizing the following criteria: GI "High" and two "YES" in druglikeness. The SwissTargetPrediction database (http://swisstargetprediction.ch/) and the UniProt database are used to identify the relevant targets.

Identification of Prospective Pharmacological Targets for Illnesses

Utilize the GeneCards database (https://www.genecards.org/), the OMIM database (https://www.omim.org/), the DisGeNet database (https://www.disgenet.org/), and the TDD database (https://db.idrblab.net/) to search for the phrase "allergic rhinitis". Consolidate and eliminate duplicates from various databases to get AR-related targets. Utilize the bioinformatics platform (http://www.bioinformatics.com.cn/) to ascertain possible XBY intervention targets for AR.

PPI Network and Principal Target Screening

Import the prospective XBY intervention targets on AR into the STRING database (https://cn.string-db.org/), selecting "Homo sapiens" as the biological species and setting the confidence level above 0.4. Retain all other options at their default settings. Please obtain the PPI network model and import it into Cytoscape 3.10.0. Use the Centiscape 2.2 plugin for topological analysis. Identify and select the primary core targets based on topological metrics, including degree (D), betweenness centrality (BC), and closeness centrality (CC).

Development of the "Drug Component–Intersection Target–Disease" Network

The potential XBY intervention targets in AR were imported into Cytoscape version 3.10.0. The CentiScape 2.2 plugin was used to conduct topological network analysis, identify core drug components, and produce a visual network diagram illustrating the relationships among drug components, intersection targets, and diseases.

GO and KEGG Enrichment Analysis

Import the target genes into the DAVID database (https://david.ncifcrf.gov/), select "Homo sapiens", Set the threshold at $p< 0.05$, and conduct GO and KEGG enrichment analysis. The results were organized in descending order according to the $-\log_{10}$ (P-value) values, and the top 15 entries were chosen. Visualization was conducted using the bioinformatics platform (http://www.bioinformatics.com.cn/).

Experimental Validation

Experimental Medication

Ephedra herba 8 g, *Hedysarum multijugum maxim* 15 g, *Saposhnikoviae radix* 10 g, *Notopterygii rhizome et radix* 12 g, *radix Paeoniae rubra* 15 g, *Cortex moutan* 15 g, *Tribulifructus* 10 g, *radix Rehmanniae* 15 g, *Bombyx batryticatus* 10 g, *Crassostrea gigas* 20 g, and *Atractylodes macrocephala koidz* 10 g. All herbal slices were obtained from the Chinese Medicine Pharmacy at The First Affiliated Hospital of Anhui University of CM. Incorporate eight volumes of purified water, boil using high heat, and allow the calcined oyster shell to simmer for 20 minutes. Incorporate the remaining herbs with eight times the volume of purified water. Bring the mixture to a boil over high heat, then reduce the heat to low and allow it to simmer for 40 minutes. Strain the decoction; add purified water to the residual herbs until they are submerged by 3 cm. Bring the mixture to a boil over high heat, then reduce to low heat and simmer for 40 minutes. Filter using cheesecloth to acquire the decoction, merge with the initial decoction, and concentrate to a 1.54 g/mL density. Refrigerate at 4°C for future use. Cetirizine Hydrochloride Tablets (Specification: 10 mg * 18 tablets, 20240301) are obtained from the Western Medicine Pharmacy at The First Affiliated Hospital of Anhui University of CM.

Animals

Forty-eight male SPF-grade BALB/c mice, aged 6 to 8 weeks and weighing 22 ± 2 g, were acquired from Hangzhou Ziyuan Laboratory Animal Technology Co., Ltd. The license number for the experimental animal is SCXK (Zhejiang) 2019–0004. The mice were maintained in the SPF animal facility at the Animal Housing Centre of Anhui University of Chinese Medicine for one week for standard housing and acclimatization, with unrestricted access to food and water and a 12-hour light-dark cycle. Approval number for animal ethics: AHUCM-mouse-2024020.

Development of an AR Model

Forty-eight SPF-grade BALB/c male mice were numbered sequentially from 1 to 48 and randomly assigned to 6 groups (n=8) using a random number table: the control group, the model group, the low-dose XBY group (XBY-L), the medium-dose XBY group (XBY-M), the high-dose XBY group (XBY-H), and the cetirizine hydrochloride group (CH). Construction of an AR model: Induction exposure (Days 1–14): Make a solution by mixing 0.3 mg of OVA and 30 mg of $Al(OH)_3$ in 1 mL of 0.9% NaCl. Apply intraperitoneal injections (i.p.) to the Model, XBY-L, XBY-M, XBY-H, and CH groups every other day for a total of seven administrations. The control group will receive 1 mL of 0.9% NaCl solution. Eliciting exposure (Days 15–28): Prepare a 5% OVA solution by dissolving 10 mg of OVA in 2 mL of 0.9% NaCl. Administer 0.05 mL to each nasal cavity of the Model, XBY-L, XBY-M, XBY-H, and CH groups once daily for 7 days, with an extra dosage on day 8, every other day. The control group was administered 0.05 mL of 0.9% NaCl solution in each nasal cavity. Administration phase: Days 15–28, one hour before sensitization, administered via gastric gavage using the body surface area equivalent dose method (with a reference human body weight of 60 kg). Prepare 1-fold, 2-fold, and 4-fold equivalent doses and administer them to the XBY-L, XBY-M, and XBY-H groups with XBY concentrate at 154 mg/(kg·d), 308 mg/(kg·d), and 616 mg/(kg·d) in a volume of 0.4 mL. The CH group received a cetirizine hydrochloride solution at a concentration of 1 mg/(kg·d) in a volume of 0.4 mL. The control and model groups received 0.4 mL of 0.9% NaCl for 14 days.

Sample Preparation

Anesthesia: 24 hours following the final sensitization on day 28, anesthetize 48 mice (1% sodium pentobarbital, 10 mL/kg, intraperitoneally) and euthanize them via cervical dislocation. Serum Preparation: Blood was obtained from the orbital vein, centrifuged at 3000 rpm for 15 minutes (5242, Eppendorf AG), and the supernatant was preserved at −80°C. Nasal Mucosa Processing: Bilateral nasal turbinates and nasal septum mucosa were harvested, fixed in a 4% paraformaldehyde solution, embedded in an optimal cutting temperature (OCT) compound, and preserved at −80°C for future analysis. Preparation of cell suspension: Remove the mucosa from both nasal turbinates and the nasal septum of mice, rinse with PBS (37538, Thermo Fisher), and section into minute fragments. Incorporate a 0.25% trypsin solution (25200072, Thermo Fisher) and a 0.1% collagenase IV combination (1 mL), then incubate at 37°C with gentle agitation for 20 minutes. Incorporate 10% fetal bovine serum (B265994, Aladdin) to halt the reaction; filter using a 150 μm filter and collect the filtrate; perform gradient centrifugation at 1000 rpm for 5 minutes and discard the supernatant. Resuspend in PBS, gradually layer onto the lymphocyte separation medium (ABS-9518, Absin) in equal volumes, and centrifuge at 2500 rpm for 20 minutes. Aspirate the interface layer comprising individual cells, wash twice with PBS, centrifuge at 1000 rpm for 5 minutes, stain with trypan blue (T6275, Macklin) to assess cell viability ≥95%, and modify the cell density accordingly.

Scoring of Allergic Symptoms in Mice

Monitor and document any allergy-related symptoms in mice within 30 minutes post-sensitization, including sneezing, rhinorrhea, and nasal pruritus. Consult the evaluation standards set by Zhao Xiu-Jie et al. Reference:[20] Sneezing: 1 point (1–3 occurrences), 2 points (4–10 occurrences), 3 points (exceeding 10 occurrences); rhinorrhea: 1 point (discharge reaching the anterior nares), 2 points (discharge surpassing the anterior nares), 3 points (discharge flowing over the face); nasal pruritus: assess the frequency of nasal scratching, 1 point (2–3 instances), 2 points (4–5 instances), 3 points (≥5 instances). The final score is determined by summing the individual scores, with a total exceeding 5 points, which means effective modeling.

HE Staining

Quickly stabilize the nasal mucosal tissue in 4% paraformaldehyde, then wash it meticulously with PBS. Next, dehydrate, clarify, and embed in paraffin. Prepare tissue sections and thereafter heat them at 60°C in a carbon-fired slide heater for 30 minutes before use. Wax was eliminated using xylene (3 × 5 min), dried with a 100% ethanol solution (3 × 5 min), and cleaned with PBS three times. The slides were cleaned and stained with a hematoxylin-eosin solution (R20570, YUANYE), dried, and mounted with a neutral mounting medium. Histological alterations in the nasal mucosa and infiltration of inflammatory cells were seen microscopically (CX41, Olympus C).

Toluidine Blue Staining

Paraffin-embedded areas were deparaffinized and rehydrated, using a procedure identical to the HE processes. A 0.5% toluidine blue staining solution (R20298, YUANYE) was employed for staining at ambient temperature in the absence of light for 20 minutes. The portions were briefly rinsed with double-distilled water to eliminate surplus dye. The slides were subsequently immersed in 70% ethanol and agitated for 5–10 seconds until the backdrop became translucent, revealing the MC granules as distinct purple-red structures. The slides were dehydrated using 95% ethanol for 30 seconds, followed by 100% ethanol at two intervals of one minute each, and thereafter sealed with neutral gum. The invasion and expression of MC were noted.

ELISA Assay for Serum Concentrations of Relevant Factors

The ELISA assay quantifies the levels of TNF-α (JYM0218Mo, JiYinMei), IL-6 (JYM0012Mo), OVA-sIgE (JYM0218Mo), IgE (JYM0552Mo), VCAM-1 (JYM0251Mo), ICAM-1 (JYM0003Mo), and COX-2 (JYM0618Mo) in murine serum. The assay was conducted according to the ELISA kit protocols, which encompassed sample dilution, sample addition, enzyme labeling, and measurement of the absorbance of inflammatory components in each well.

WB Assessment of Associated Protein Concentrations

WB test measured the amounts of several proteins: PI3K (1:1000), p-PI3K (1:1000), AKT (1:1000), p-AKT (1:2000), Ikkβ (1:1000), p-Ikkβ (1:2000), NF-kB (1:5000), p-NF-kB (1:1000), Bax (1:5000), Bcl-2 (1:1000), Caspase-3 (1:2000), and Cleaved-Caspase-3 (1:1000). A random number table method was employed to choose nasal mucosa randomly from three mice per group. Six hundred microliters of RIPA lysis buffer (P0013B, BeyoTime) were homogenized on ice for thirty minutes. Centrifuge at 11,000 rpm for 15 minutes, and collect the supernatant. Quantify the total protein contents with the BCA assay kit (P0012, Beyotime). Incorporate protein loading buffer, immerse in a boiling water bath for 15 minutes, and completely denature the protein. Separation by SDS-PAGE electrostatic precipitation Transfer the proteins molecules across a PVDF membrane (S917800, Merck Millipore), check how well the transfer worked using a pre-stained protein marker (26616, Thermo Fisher), mix in 5% non-fat milk powder and let it sit at ambient temperature for one hour to inhibit any undesired binding, then dilute the primary antibody (1:1000) with PBST, let it sit at 4°C overnight, and perform three washes. Rinse the membrane with PBST, add HRP-conjugated secondary antibody (1:20,000) (goat anti-mouse IgG (G709256, Macklin), goat anti-rabbit IgG (G709257, Macklin)), and incubate at room temperature in a shaking incubator for 1.2 hours, followed by three washes with PBST. Chemiluminescence was identified with a high-sensitivity ECL kit (34094, Thermo Fisher). Electrophoresis unit: EPS300; electrophoresis chamber: VE-180; film transfer unit: VE-186, Tanon. The grayscale values for each band were obtained using ImageJ software.

Detection of ROS Using FCM

Modify the concentration of each of the cell suspensions from the preceding stage to (1–10) × 10^6 cells/mL, thereafter, incorporating the DCFH-DA probe (reactive oxygen species detection reagent kit, S0033S, Beyotime) at an exposure level of 10 μmol/L. Incubate at 37°C in darkness for 30 minutes, gently mixing every 10 minutes throughout the incubation period. Two rinses with PBS are performed, followed by an analysis of ROS using a flow cytometer (CytoFLEX, Beckman). The data analysis was conducted using FlowJo v10.

FCM Analysis of Cellular Apoptosis

Modify the concentration of the cell suspension derived from the preceding step to (1–10) × 10^5 cells/mL. Transfer 500 μL of the cell suspension into each tube, incorporate five μL of Annexin V-FITC and 10 μL of propidium iodide (PI) (Annexin V-FITC/PI apoptosis kit, Multisciences), incubate at room temperature in a light-free environment for 20 minutes, and subsequently conduct FC to assess the apoptosis levels. Conduct analysis utilizing FlowJo v10.

Statistical Techniques

Statistical analysis was performed using GraphPad Prism 10.3.0 software. Quantitative data were presumed to adhere to a normal distribution with uniform variances. Results are presented as mean ± standard deviation (x ± s). Comparisons among various groups were conducted using one-way ANOVA, with $p < 0.05$, indicating statistical significance.

Results

Outcomes from Network Pharmacology

Active Components of the Pharmaceutical Agent and Associated Targets

Following the screening of *Ephedra herba, Hedysarum multijugum maxim, Saposhnikoviae radix, Notopterygii rhizome et radix, radix Paeoniae rubra, Cortex moutan, Tribulifructus, radix Rehmanniae, Bombyx batryticatus, Crassostrea gigas*, and *Atractylodes macrocephala koidz*, a total of 41 active components were identified. The list included nine from *Ephedra herba*, 11 from *Hedysarum multijugum maxim*, seven from *Saposhnikoviae radix*, seven from *Notopterygii rhizome et radix*, one from *radix Paeoniae rubra*, three from *Cortex moutan*, one from *Tribulifructus*, one from *radix Rehmanniae*, one from *Atractylodes macrocephala koidz*, and none from *Bombyx batryticatus* or *Crassostrea gigas*. All drug targets were consolidated, and duplicates were eliminated, resulting in 567 unique targets.

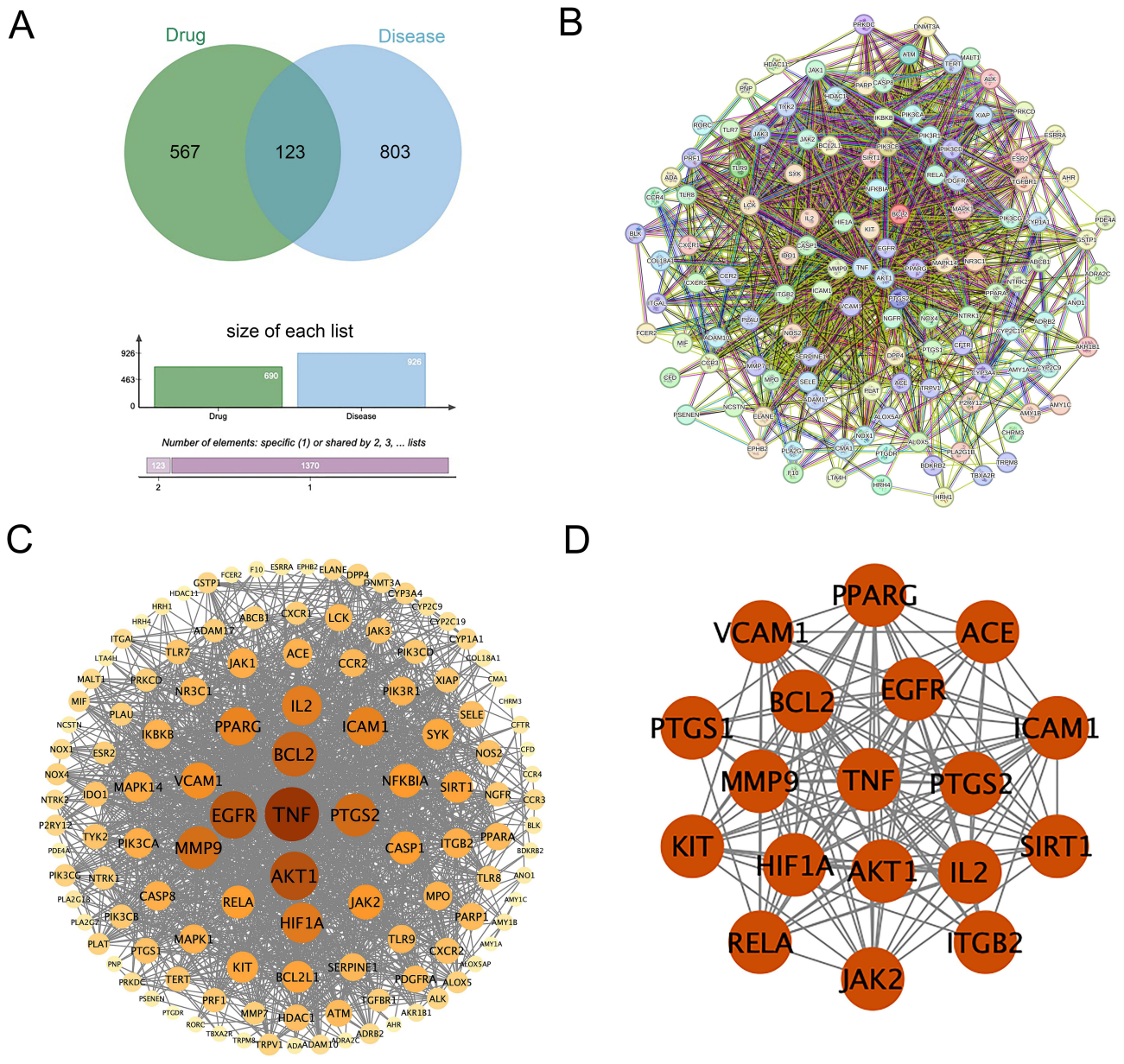

Figure 1 Network pharmacology-related diagram. (**A**) Venn diagram showing the overlap between drug (XBY) and disease (AR) targets, with 123 intersecting targets. (**B**) Protein-protein interaction network diagram. (**C**) Visual protein-protein interaction network diagram. The larger and darker the circle, the greater its degree value. (**D**) The 18 core targets associated with AR.

Prospective Pharmacological Targets for Disease Intervention

Targets for the disease were found in four databases: GeneCards, OMIM, DiGeNet, and TDD, and duplicate entries were eliminated to yield 800 targets associated with AR. Drug and illness targets were uploaded to an online bioinformatics analysis and visualization cloud platform (http://www.bioinformatics.com.cn/) to discover 123 target intersections, as illustrated in Figure 1A.

PPI Network Diagram and Visualization of the Core Target Network for Diseases

The overlapping targets were imported into the STRING database (https://cn.string-db.org/), with the species designated as "Homo sapiens" and a confidence threshold of 0.4, to generate the PPI network model diagram (Figure 1B). The overlapping targets were subsequently loaded into Cytoscape 3.10. The software produced a network diagram including 122 nodes and 1446 edges. Utilizing the integrated topological analysis plugin in Centicape 2.2, we constructed the PPI visualization network diagram (Figure 1C) predicated on C value > 0.0042, B value ≥ 120.13, and D value ≥ 23.7, identifying 18 key targets, as illustrated in Table 1 and Figure 1D.

Visualization of the "Drug Component-Intersection Target-Disease" Network

We import the intersection of targets and the active ingredient targets into Cytoscape 3.10.0 software to generate a network diagram including 170 nodes and 987 edges. We utilize topological analysis to ascertain the fundamental drug components and generate a visualization of the interaction among "drug components-intersecting targets-disease" (Figure 2). The top active ingredients identified were Genkwanin (MOL005573, 27), Calycosin (MOL000417, 24), Kaempferol (MOL000422, 24), and Luteolin (MOL000006, 24), which came from *Ephedra herba, Hedysarum multi-jugum maxim*, and *Cortex moutan* (Table 2 and Figure 3).

GO and KEGG Enrichment Analysis

One hundred twenty-three intersecting target genes were uploaded to the DAVID database, with the species designated as "Homo sapiens" for Gene Ontology functional analysis ($p < 0.05$), resulting in 550 Biological Process (BP) entries, 66 Cellular Component (CC) entries, and 121 Molecular Function (MF) entries. The results were organized in descending order according to the -log10 P (P-value). The findings indicated that the pertinent target genes were predominantly associated with BP, such as inflammatory response, calcium signaling, and reaction to external stimuli; CC, including cell membrane, extracellular membrane, and cell surface; and MF, encompassing protein binding, enzyme binding, and protein tyrosine kinase activation.

Table 1 Information on 18 Disease Core Targets

Target Gene	Degree	Betweenness Centrality	Closeness Centrality
TNF	92	2081.381	0.00629
AKT1	79	820.830	0.00581
EGFR	77	952.184	0.00574
BCL2	71	533.459	0.00552
PTGS2	67	971.295	0.00543
MMP9	66	503.235	0.00556
HIF1A	61	340.137	0.00541
IL2	59	642.877	0.00518
ICAM1	57	293.136	0.00510
PPARG	56	632.082	0.00518
VCAM1	51	228.176	0.00498
JAK2	48	162.604	0.00476
RELA	44	213.871	0.00472
SIRT1	41	250.297	0.00467
KIT	40	146.724	0.00459
ITGB2	36	245.355	0.00450
ACE	35	533.271	0.00463
PTGS1	27	584.156	0.00442

https://doi.org/10.2147/JIR.S550848

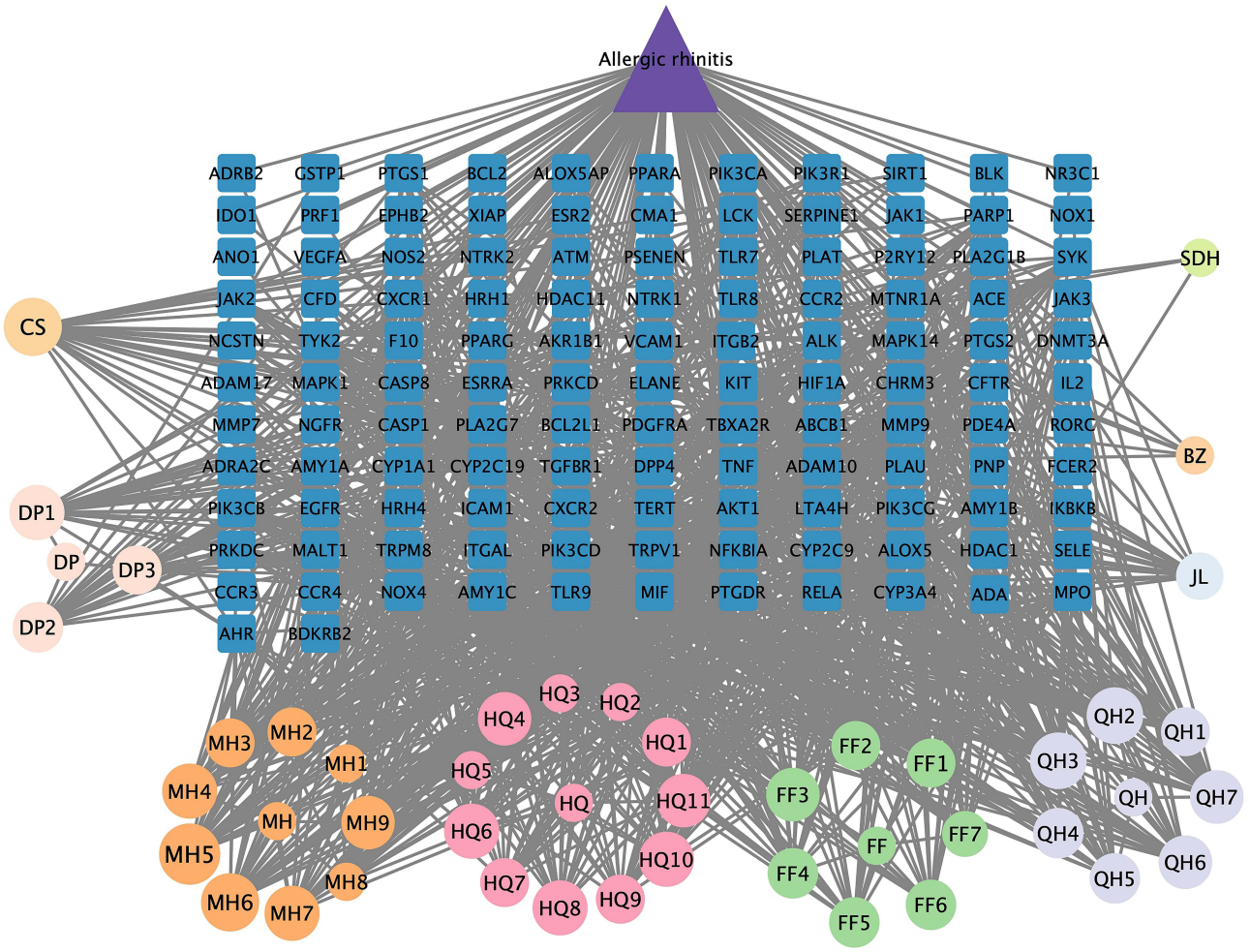

Figure 2 A visual depiction of the "drug component-intersection target-disease" network. Circles represent components of Chinese herbal medicine in XBY; triangles represent the diseases (AR); and squares represent disease proteins. The larger a circle, the greater the amount of that active ingredient derived from the herb.

The 10 highest entries from BP, CC, and MF were chosen and illustrated in a bar chart, as depicted in Figure 4A. KEGG enrichment analysis revealed 152 signaling pathway entries ($p < 0.05$). The findings indicated that the pathways were predominantly associated with the phospholipase-3 kinase/protein kinase B signaling pathway (hsa04151: PI3K/AKT signaling pathway), the apoptosis pathway (hsa04210: Apoptosis), and the NFκB signaling pathway (hsa04064: NF-kappa B signaling pathway). The 15 foremost paths were chosen according to decreasing -log10 (P-value) values and illustrated as a bubble diagram, as depicted in Figure 4B.

Table 2 Information on Four Core Drug Active Ingredients

Ingredients	Herb Name	No.	Mol ID	OB	DL	Degree
Genkwanin	*Ephedra herba*	MH6	MOL005573	37.13	0.23	27
Calycosin	*Hedysarum multijugum Maxim.*	HQ8	MOL000417	47.75	0.24	24
Kaempferol	*Cortex Moutan/Radix Paeoniae Rubra/ Ephedra herba/Hedysarum multijugum Maxim*	DP1/MH4/ HQ10	MOL000422	41.88	0.24	24
Luteolin	*Ephedra herba*	MH7	MOL000006	36.16	0.24	24

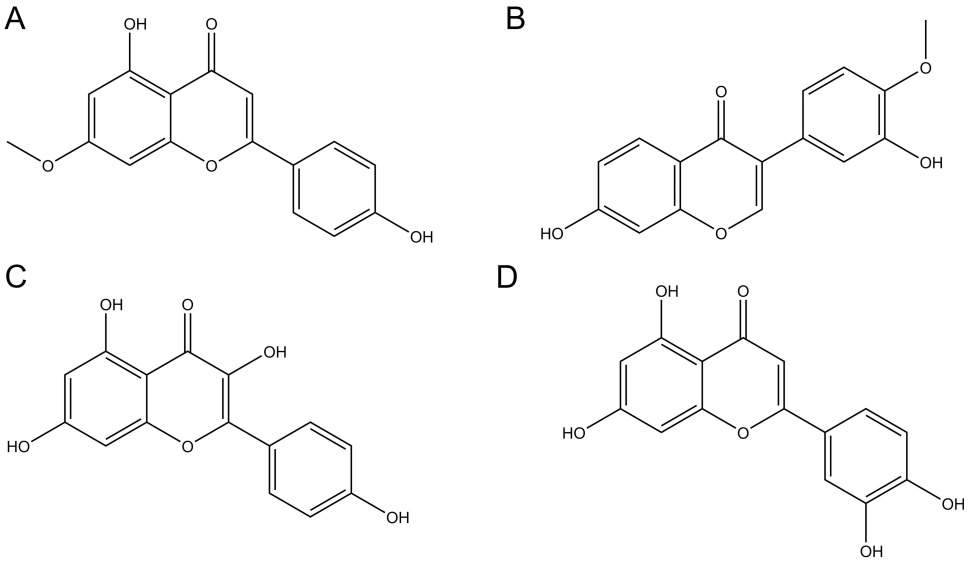

Figure 3 Chemical structures of the 4-core drug active ingredients: (**A**) Genkwanin (**B**) Calycosin (**C**) Kaempferol (**D**) Luteolin.

Empirical Findings

Observation and Documentation of Allergy Symptoms in AR Mice

The model group exhibited a statistically noteworthy rise in the allergy symptom score compared to the control group ($p < 0.01$). The XBY-L, XBY-M, XBY-H, and CH groups demonstrated a statistically significant decrease in allergy symptom scores relative to the model group ($p < 0.01$). Refer to Figure 5. Figure 6 illustrates the procedure for constructing the mouse model.

HE and Toluidine Blue Staining of Mouse Nasal Mucosal Tissue Morphology

HE staining results indicated that, compared to the control group, the model group displayed pronounced nasal mucosal congestion and edema, thickened epithelial tissue with partial detachment, disorganized cellular arrangement, lymphocyte aggregation, eosinophil infiltration, and proliferation of cup-shaped cells. In contrast to the model group, XBY-L, XBY-M, XBY-H, and CH groups exhibited significantly diminished nasal mucosal tissue congestion and edema, relatively intact epithelial tissue, and a substantial reduction in eosinophils. Furthermore, submucosal inflammatory cell infiltration in the Model, XBY-L, XBY-M, and XBY-H groups progressively decreased, as illustrated in Figure 7.

The results of toluidine blue staining indicated that MC exhibited a blue-purple coloration. MC infiltration was significantly elevated in the model group compared to the control group; however, it was markedly diminished in the XBY-L, XBY-M, XBY-H, and CH groups relative to the model group, as illustrated in Figure 8.

EILSA Assessment of Pertinent Factor Expression in the Serum of Mice Across Each Group

The model group had markedly elevated levels of OVA-sIgE, Total-IgE, IL-6, TNF-α, and COX-2 in their serum compared to the control group ($p < 0.01$). The XBY-L, XBY-H, and XBY-H groups had markedly reduced levels of Total-IgE, OVA-sIgE, IL-6, TNF-α, and COX-2 in their serum compared to the model group ($p < 0.05$, $p < 0.01$), as illustrated in Figure 9. The model group had significantly elevated levels of ICAM-1 and VCAM-1 in their serum compared to the control group ($p < 0.01$). The XBY-L, XBY-M, XBY-H, and CH groups had significantly reduced blood levels of total ICAM-1 and VCAM-1 compared to the model group ($p < 0.05$, $p < 0.01$), as illustrated in Figure 10.

Western Blot Analysis of Protein Expression Associated with the PI3K/AKT/NFκB Signaling Pathway in the Nasal Mucosa of Each Group

The model group exhibited significantly higher levels of p-PI3K/PI3K, p-AKT/AKT, p-NF-κB/NF-κB, and p-IκBα/IκBα proteins in the nasal mucosa compared to the control group ($p < 0.01$). XBY-L exhibited no statistical significance relative to the model group regarding p-PI3K/PI3K, p-AKT/AKT, p-n-p65/c-p65, and p-Ikkβ/Ikkβ ratios. XBY-M exhibited no statistical significance relative to the model group regarding p-Ikkβ/Ikkβ while demonstrating

 https://doi.org/10.2147/JIR.S550848

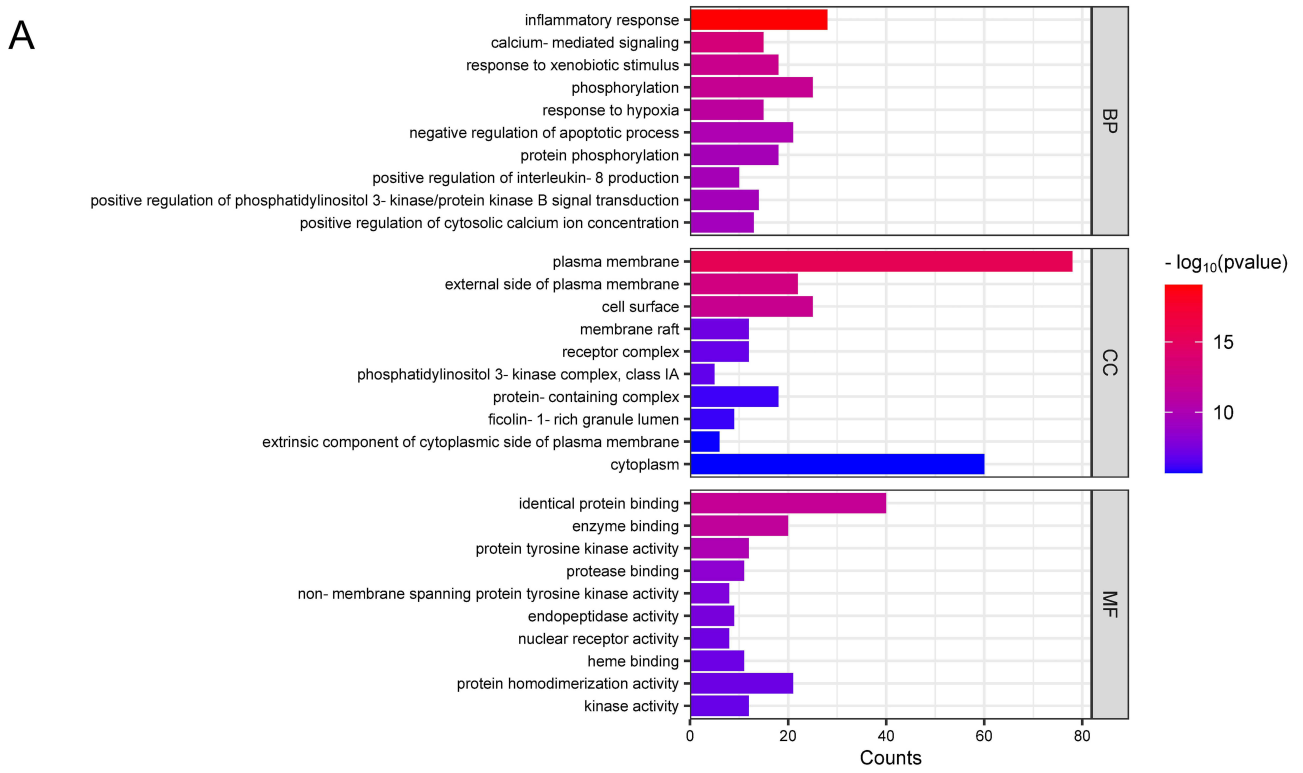

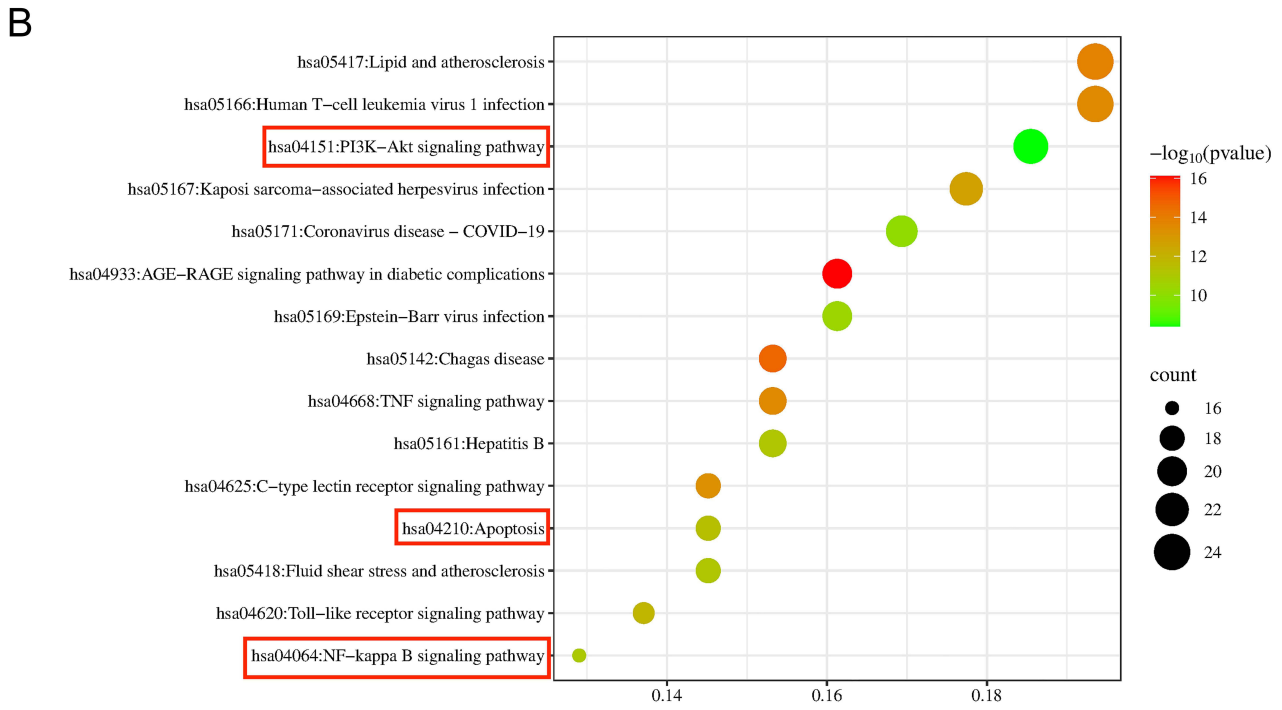

Figure 4 GO and KEGG enrichment analysis results. (**A**) GO enrichment analysis bar chart. The X-axis shows the number of target genes, and the Y-axis shows the target gene category. (**B**) KEGG enrichment analysis bubble chart. The X-axis represents the ratio of all genes in each pathway, and the Y-axis represents important pathways. The color and size of the bubbles represent the P-value and the number of related targets, respectively. The more genes enriched in a pathway, the larger the bubble. The color reflects the P-value: the smaller the P-value, the larger the -$\log_{10}$(P-value), and the redder the bubble. The content within the red box represents the three signaling pathways identified through GO and KEGG enrichment analysis. These are hsa04151: PI3K-AKT signaling pathway, hsa04210: Apoptosis, and hsa04064: NF-kappa B signaling pathway.

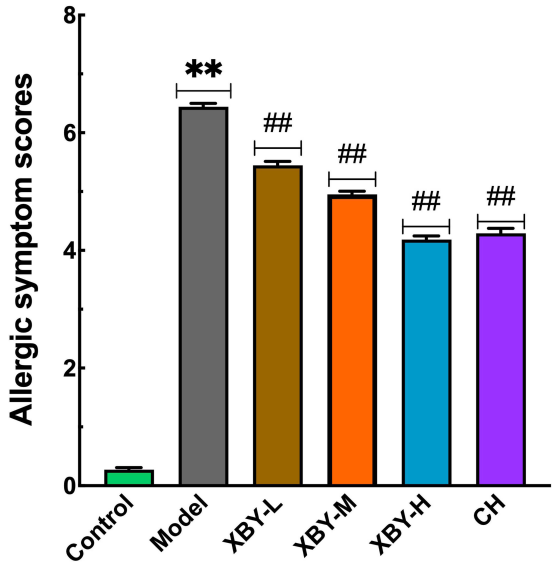

Figure 5 Mouse allergic symptom scores. A score ≥5 indicates successful modeling. **p<0.01 vs the control group, ##p<0.01 vs the model group.

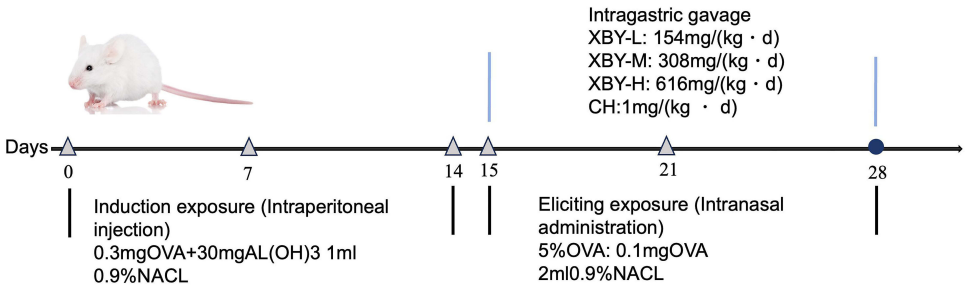

Figure 6 AR mouse model construction and XBY administration procedure.

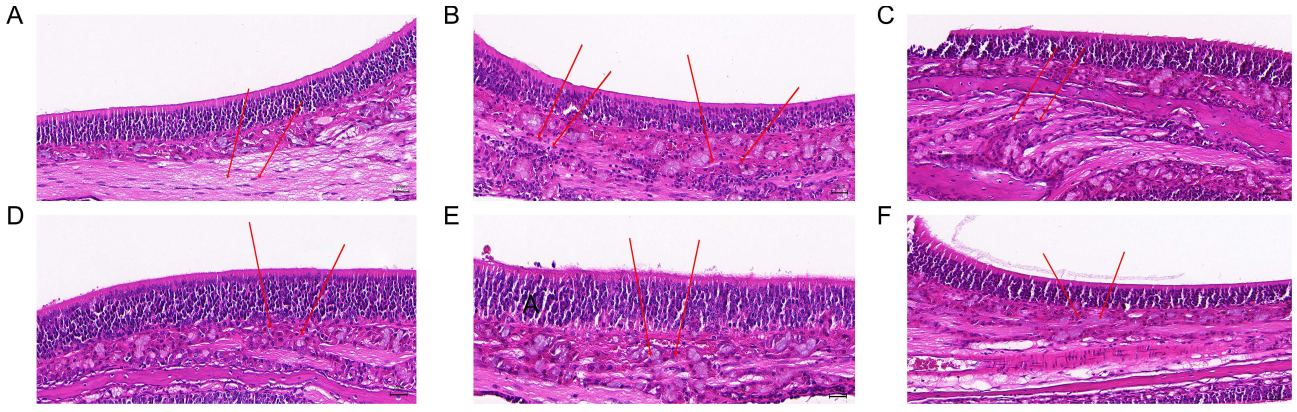

Figure 7 Morphology of nasal mucosal tissue in each group (n=8) of mice under HE staining (400×, 20 μm). The area indicated by the red arrow shows eosinophil infiltration. (**A**) The control group exhibited no obvious nasal mucosal edema or hyperemia, with a clearly organized cellular arrangement and no detectable eosinophil infiltration. (**B**) The model group showed nasal mucosal hyperemia and edema, thickened epithelial tissue with localized desquamation, disorganized cellular arrangement, and marked eosinophil infiltration. (**C**) The XBY-L group showed no significant reduction in nasal mucosal hyperemia and edema, with disorganized cellular arrangement and marked eosinophil infiltration. (**D**) The XBY-M group showed mild reduction in nasal mucosal hyperemia and edema, improved cellular arrangement, and a slight decrease in eosinophil infiltration. (**E**) The XBY-H group showed a clear reduction in nasal mucosal hyperemia and edema, with more regular cellular arrangement and a notable decrease in eosinophil infiltration. (**F**) The CH group showed marked reduction in nasal mucosal hyperemia and edema, with more orderly cellular arrangement and decreased eosinophil infiltration.

https://doi.org/10.2147/JIR.S550848

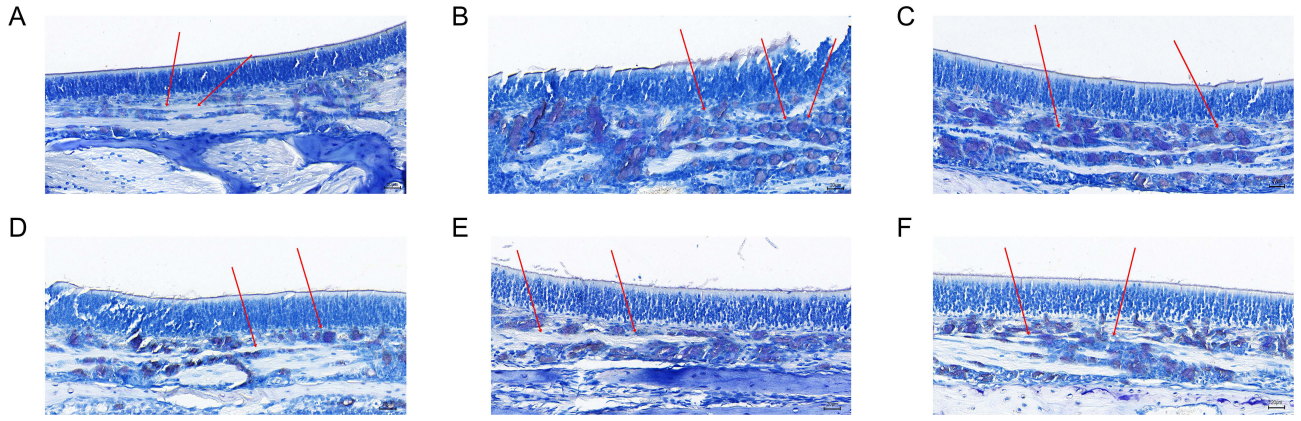

Figure 8 Morphology of nasal mucosal tissue in each group (n=8) of mice under toluidine blue staining (400×, 20 μm). Mast cells appear blue-violet. The area indicated by the red arrow shows mast cell infiltration. (**A**) The control group exhibited no notable mast cell infiltration. (**B**) The model group showed significant mast cell infiltration. (**C**) The XBY-L group showed marked mast cell infiltration. (**D**) The XBY-M group showed a slight reduction in mast cell infiltration. (**E**) The XBY-H group showed a substantial decrease in mast cell infiltration. (**F**) The CH group showed markedly reduced mast cell infiltration.

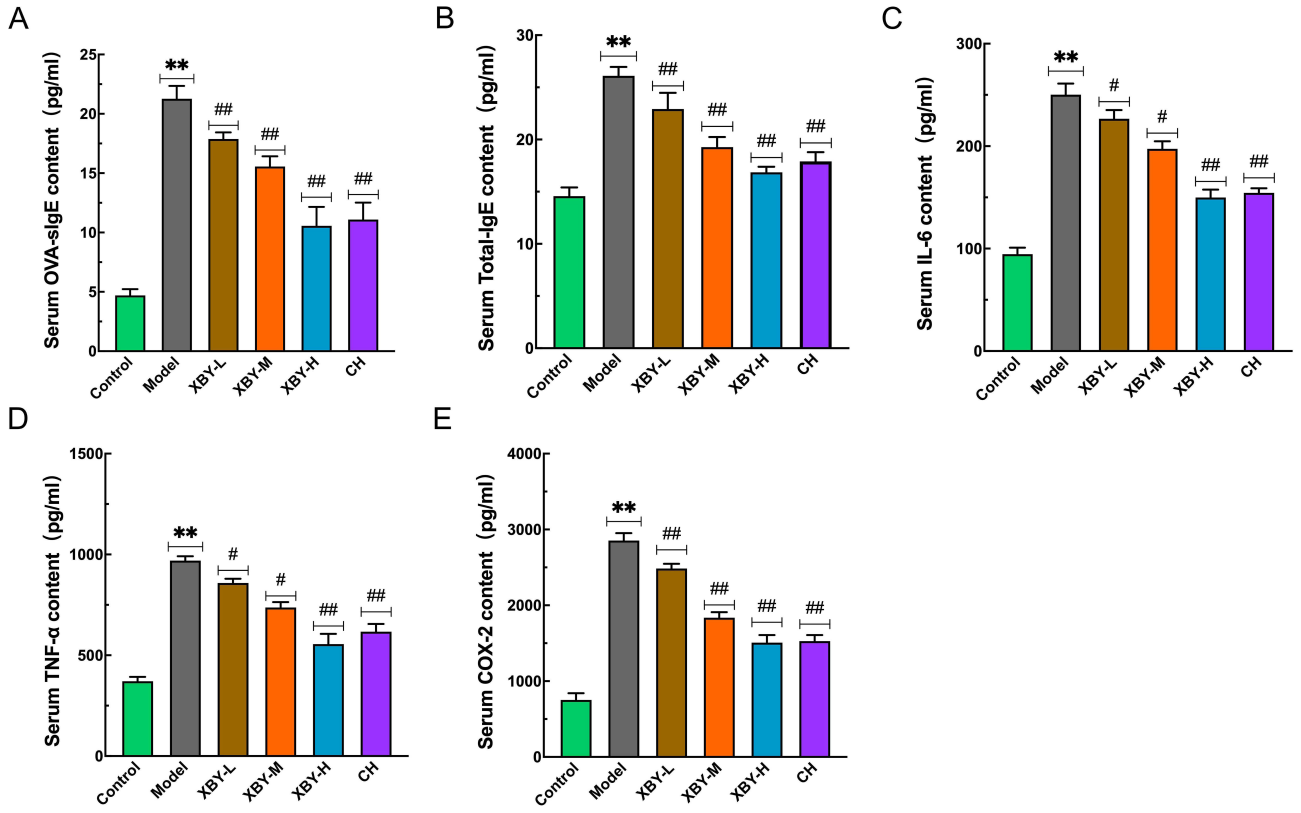

Figure 9 Statistical analysis of OVA-sIgE, total-IgE, IL-6, TNF-α, and COX-2 levels in mouse serum by ELISA. (**A**) OVA-sIgE; (**B**) Total-IgE; (**C**) IL-6; (**D**) TNF-α; (**E**) COX-2. Data are presented as means ± SD (n=8). $^{**}p < 0.01$ vs the control group, $^{\#}p < 0.05$, $^{\#\#}p < 0.01$ vs the model group.

a substantial reduction in p-PI3K/PI3K, p-AKT/AKT, and p-n-p65/c-p65 ($p < 0.05$). The XBY-H and CH groups had markedly reduced ratios of p-PI3K/PI3K, p-AKT/AKT, p-n-p65/c-p65, and p-Ikkβ/Ikkβ protein expression compared to the model group ($p < 0.05$, $p < 0.01$), as illustrated in Figures 11 and 12.

WB Study of Apoptosis-Related Protein Expression in Nasal Mucosal Cells Across All Groups

The model group showed much lower amounts of Bax, cleaved-Caspase-3, and Caspase-3 proteins ($p < 0.01$) and much higher amounts of Bcl-2 protein ($p < 0.01$) compared to the control group. There was no significant difference in Bax

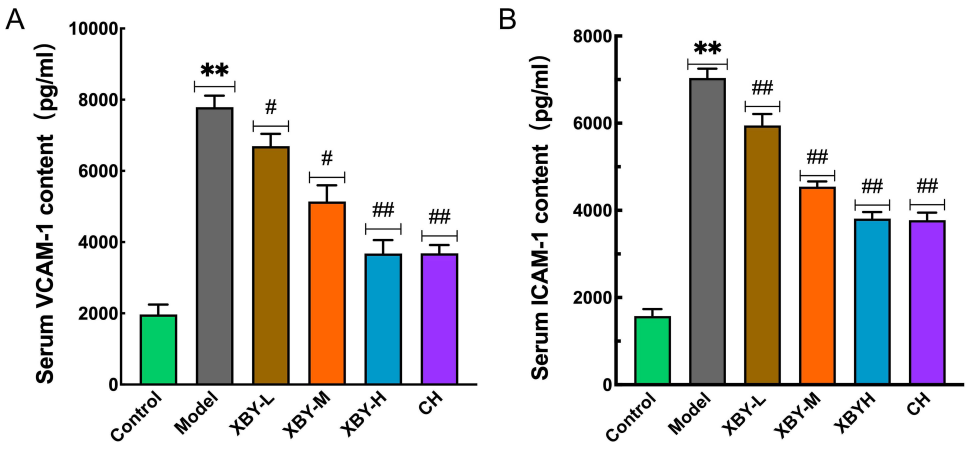

Figure 10 Statistical analysis of VCAM-1 and ICAM-1 levels in mouse serum by ELISA. (**A**) VCAM-1; (**B**) ICAM-1. Data are presented as means ± SD (n=8). $^{**}p < 0.01$ vs the control group, $^{\#}p < 0.05$, $^{\#\#}p < 0.01$ vs the model group.

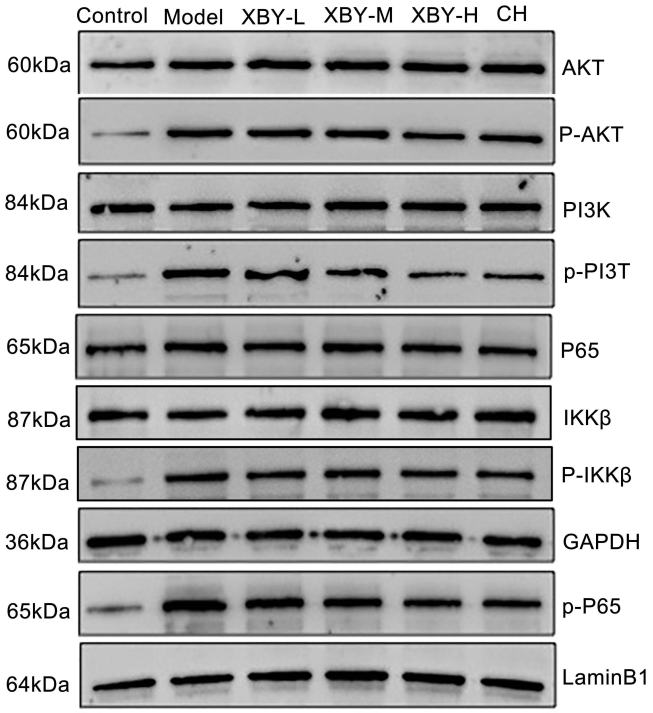

Figure 11 Expression of p-PI3K, PI3K, p-AKT, AKT, p-n-p65, c-p65, p-Ikkβ, and Ikkβ protein bands.

protein levels between the model group and the XBY-L group, but Bcl-2 protein levels were much lower ($p < 0.05$), while Cleaved Caspase-3 and Caspase-3 protein levels were significantly higher ($p < 0.05$). The XBY-M, XBY-H, and CH groups showed much lower levels of Bcl-2 ($p < 0.05$, $p < 0.01$) and much higher levels of Bax, Cleaved-Caspase-3, and Caspase-3 ($p < 0.05$, $p < 0.01$) compared to the model group, as shown in Figures 13 and 14.

FCM for the Detection of Cellular ROS Levels and Apoptosis

When compared to the control group, the ROS abundances in the nasal mucosa tissue of the model group mice were markedly elevated; conversely, the ROS levels in the nasal mucosa tissue of the XBY-L, XBY-M, XBY-H, and CH groups were dramatically reduced relative to the model group (Figure 15). Within in comparison to the control group, the model group mice exhibited a significantly elevated number of apoptotic cells in the nasal mucosa tissue; conversely, the

https://doi.org/10.2147/JIR.S550848

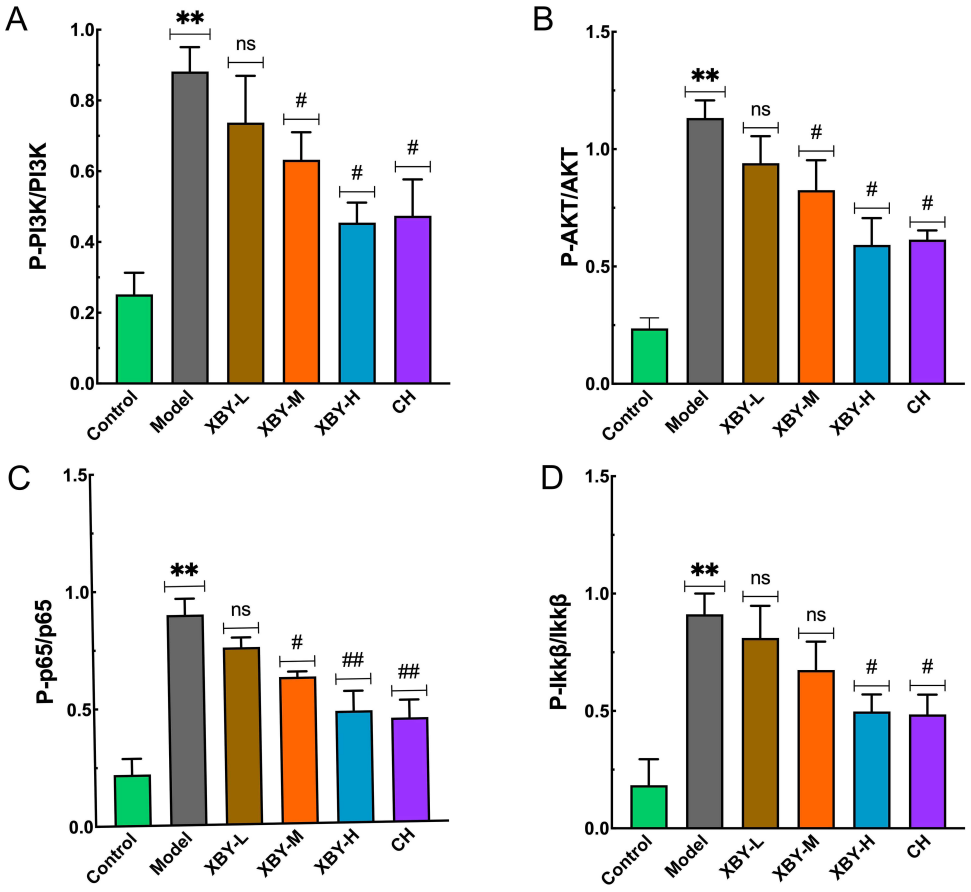

Figure 12 Statistical analysis of p-PI3K/PI3K, p-AKT/AKT, p-n-p65/c-p65, and p-Ikkβ/Ikkβ levels in the nasal mucosa of mice from each group detected by Western blot. (**A**) p-PI3K/PI3K (**B**) p-AKT/AKT (**C**) p-n-p65/c-p65 (**D**) p-Ikkβ/Ikkβ. Results data are presented as means ± SD (n=8). ns indicates no statistical significance, $^{**}p < 0.01$ vs the control group, $^{\#}p < 0.05$, $^{\#\#}p < 0.01$ vs the model group.

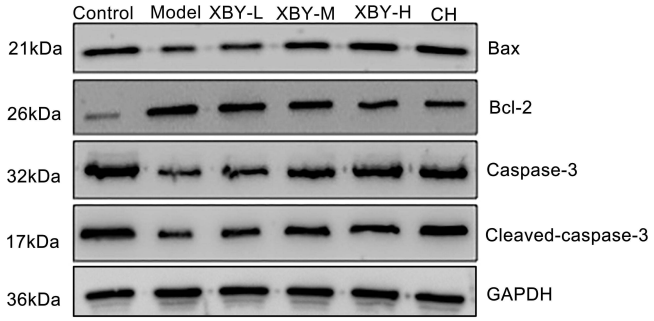

Figure 13 Western blot analysis of Bax, Bcl-2, cleaved caspase-3, and caspase-3 protein bands.

XBY-L, XBY-M, XBY-H, and CH groups demonstrated a significantly went down number of apoptotic cells in the nasal mucosa tissue relative to the model group (Figures 16 and 17).

Discussion

AR is a frequently encountered chronic inflammatory disorder in otolaryngology, characterized by symptoms involving paroxysmal sneezing, clear nasal discharge, pruritus, and obstruction. It frequently coexists with bronchial asthma. The escalation of environmental pollution has led to a continuous rise in its prevalence, adversely affecting the patients' quality of life and imposing considerable economic and medical burdens on society.[21,22] TCM has demonstrated

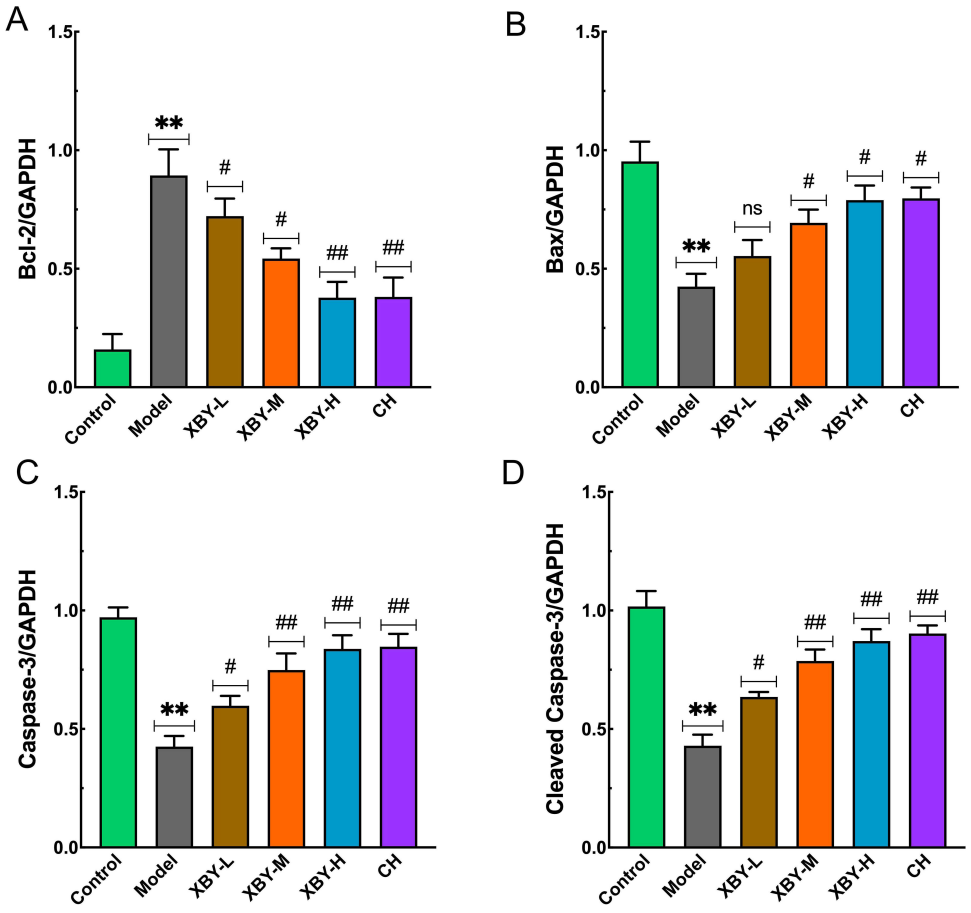

Figure 14 Statistical analysis of Bcl-2, Bax, caspase-3, and cleaved-caspase-3 levels in the nasal mucosa of mice from each group detected by Western blot. (**A**) Bcl-2; (**B**) Bax; (**C**) Caspase-3; (**D**) Cleaved-Caspase-3. Data are presented as means ± SD (n=8). ns indicates no statistical significance. $^{**}p < 0.01$ vs the control group, $^{\#}p < 0.05$, $^{\#\#}p < 0.01$ vs the model group.

promising effectiveness in treating AR by modulating several signaling pathways and regulating specific targets to suppress inflammatory responses in recent years.[23] XBY has been proven to be effective through years of clinical practice; yet, its potential mechanism of action on AR remains unclear. The present research aims to clarify the possible mechanism of action in treating AR by combining network pharmacology with animal experiments.

XBY has demonstrated efficacy throughout years of clinical practice; nonetheless, the exact mechanisms that function in AR remain uncertain. The present study intends to explore how XBY works to treat AR by combining network pharmacology and animal tests. This study utilized network pharmacology analysis to identify 123 possible targets for XBY in AR, comprising 18 core targets, such as TNF, AKT1, MMP9, BCL2, IL-2, PTGS2, VCAM-1, ICAM-1, and RELA. The principal active components of the medication are Genkwanin, Calycosin, Kaempferol, and Luteolin. GO enrichment analysis indicates that targets are predominantly localized in the cytoplasmic membrane, outer membrane, and cell surface. MF predominantly encompasses protein binding, enzyme binding, and activation of protein tyrosine kinases, whereas BP chiefly involves inflammatory response, calcium signaling, and reaction to exogenous stimuli. KEGG enrichment analysis indicated that the pathways were focused on the phosphoinositide-3 kinase/protein kinase B signaling pathway (hsa04151: PI3K/AKT signaling pathway), the apoptosis pathway (hsa04210: Apoptosis), and the NF-κB signaling pathway (hsa04064: NF-κB signaling pathway). Research shows that changing the PI3K/AKT/NFκB pathway can lower the release of cytokines like IL-6 and TNF-α, control the levels of the anti-apoptotic protein Bcl-2 and the pro-apoptotic protein Bax, and influence the process of apoptosis.[24,25] Therefore, this study hypothesizes that XBY's mechanism of action in treating AR may involve modulating the PI3K/AKT/NFκB signaling pathway to reduce the generation of cytokines such as IL-6 and TNF-α, inhibit apoptosis, and consequently enhance the inflammatory microenvironment of the nasal mucosa.

https://doi.org/10.2147/JIR.S550848

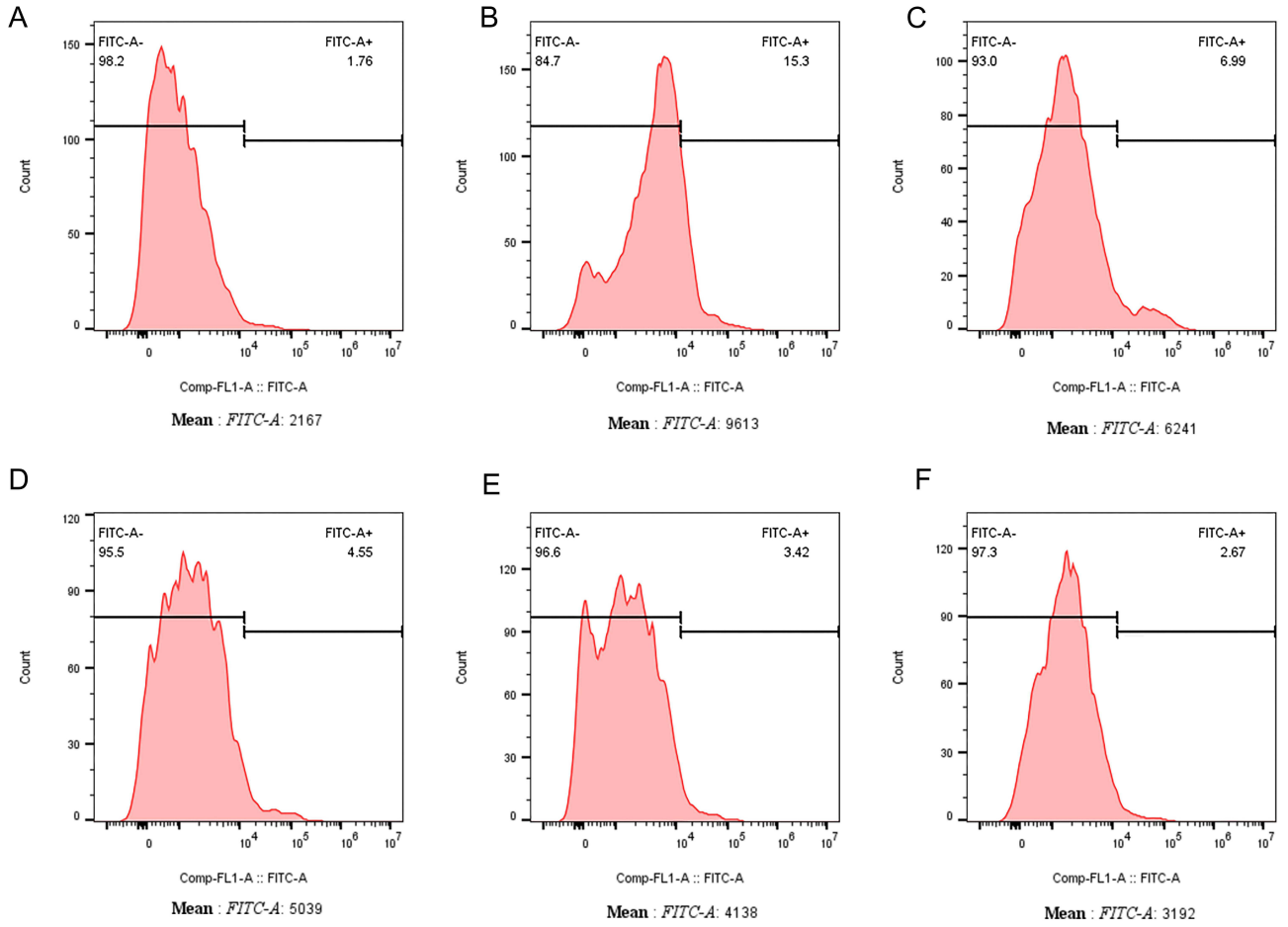

Figure 15 FCM analysis of ROS levels in nasal mucosa cells of mice in each group. (**A**) Control group; (**B**) Model group; (**C**) XBY-L group; (**D**) XBY-M group; (**E**) XBY-H group; (**F**) CH group.

AR is a hypersensitivity reaction characterized mainly by nasal mucosal symptoms. AR may be produced by the Gell and Coombs type I mechanism (mediated by allergen-specific IgE) or by a non-IgE-mediated hypersensitivity mechanism.[26,27] The pathophysiological mechanism entails nasal and airway hyperresponsiveness.[28] Nasal and airway hyperresponsiveness is intricately linked to the PI3K/AKT signaling system. Earlier studies have found that blocking the PI3K/AKT/NFκB pathway can significantly reduce inflammation in the airways and damage the protective layer in allergic asthma.[29] When exposed to outside triggers, the body produces too many ROS, leading to oxidative stress and activating pathways like PI3K/AKT. Related investigations have demonstrated that ROS directly activates PI3K and AKT and facilitates MC degranulation, producing inflammatory mediators that consist of histamine, IL-6, and TNF-α.[30,31] At the same time, active AKT phosphorylates Ikkβ, which activates the IKK complex; this complex then phosphorylates IκB, facilitating the nuclear translocation of NFκB (p65) and contributing to cellular inflammatory and immunological responses.[32] This study conducted in vivo animal experiments to evaluate whether XBY may confer therapeutic benefits for AR, potentially by modulating the ROS-mediated PI3K/AKT/NFκB signaling pathway. The current study showed that, after XBY treatment, the levels of important proteins in the PI3K/AKT/NFκB pathway, including p-PI3K/PI3K, p-AKT/AKT, p-p65/p65, and p-Ikkβ/Ikkβ, were decreased. At the same time, ROS levels dropped, suggesting that XBY might block the changes caused by ROS in the PI3K pathway, halt the AKT activation process, prevent NF-κB (p65) from entering the nucleus, and reduce cytokine production. To further support the above hypothesis, this study assessed the expression levels of AR-related effector cells and inflammatory factors.

MC and EOS are important cells involved in the unusual inflammation seen in AR. The recruitment of MC and EOS stimulates the release of cytokines, including IL-6, TNF-α, and PGD2, which aggravates inflammatory infiltration of the

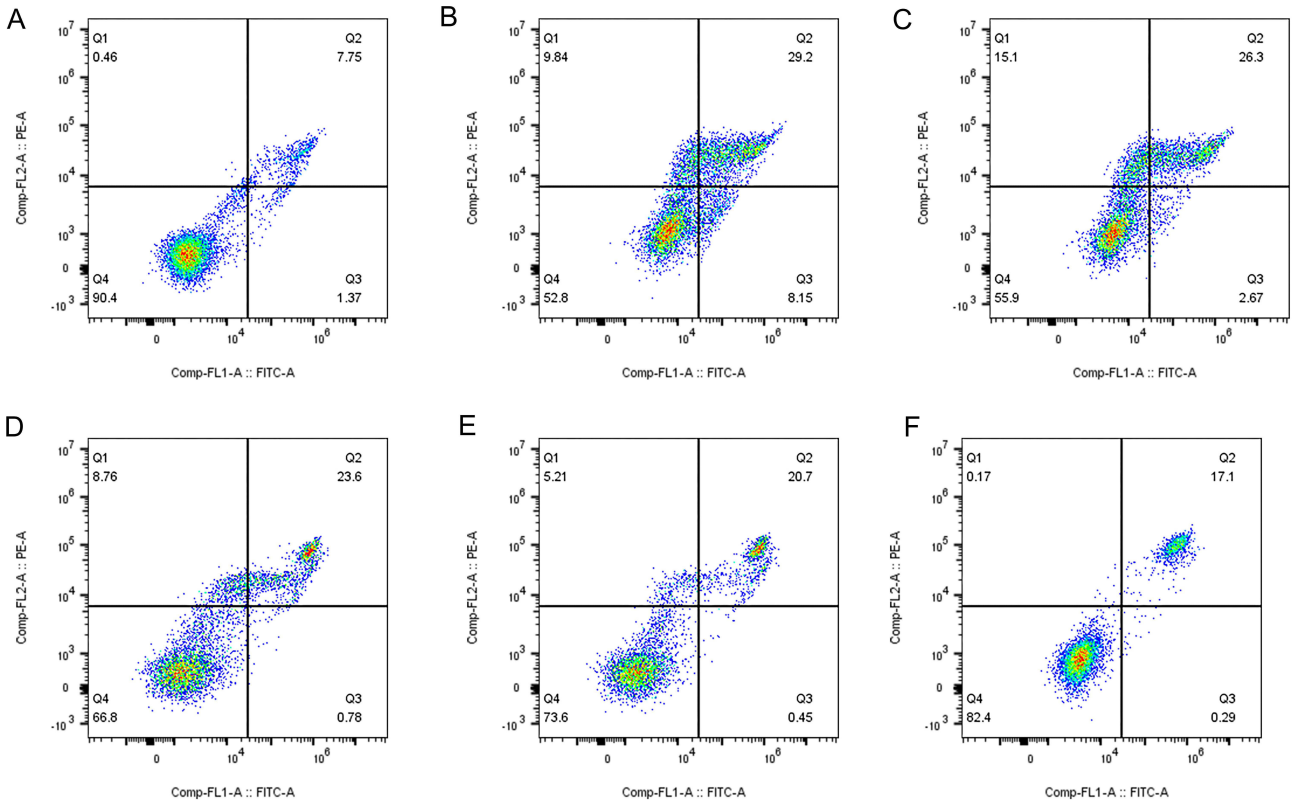

Figure 16 FCM analysis of apoptosis expression in nasal mucosa cells of mice in each group. (**A**) Control group; (**B**) Model group; (**C**) XBY-L group; (**D**) XBY-M group; (**E**) XBY-H group; (**F**) CH group.

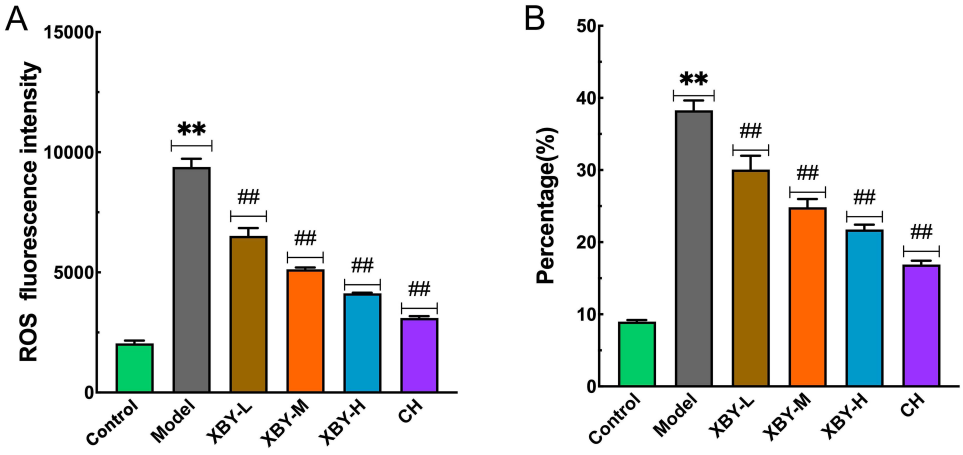

Figure 17 Statistical analysis of ROS and apoptosis levels in the nasal mucosa of mice in each group detected by FCM. (**A**) ROS; (**B**) Apoptosis. Data are presented as means ± SD (n=8). $^{**}p<0.01$ vs the control group, $^{\#\#}p<0.01$ vs the model group.

nasal mucosa and compromises the nasal mucosal barrier.[33,34] The movement of monocytes and eosinophils is helped and controlled by intercellular adhesion molecules ICAM-1 and VCAM-1.[35] ICAM-1 and VCAM-1 facilitate the adherence and infiltration of EOS to vascular endothelial cells, intensifying chronic airway inflammation, and are implicated in the regulation of physiological activities, including inflammatory and immunological responses in chronic airway inflammation.[36] Their expression is augmented by enhancing vascular endothelial cell permeability.[37] Research shows that in allergic conditions like asthma and AR, histamine, IL-6, and TNF-α produced by MC can be effectively reduced by

https://doi.org/10.2147/JIR.S550848

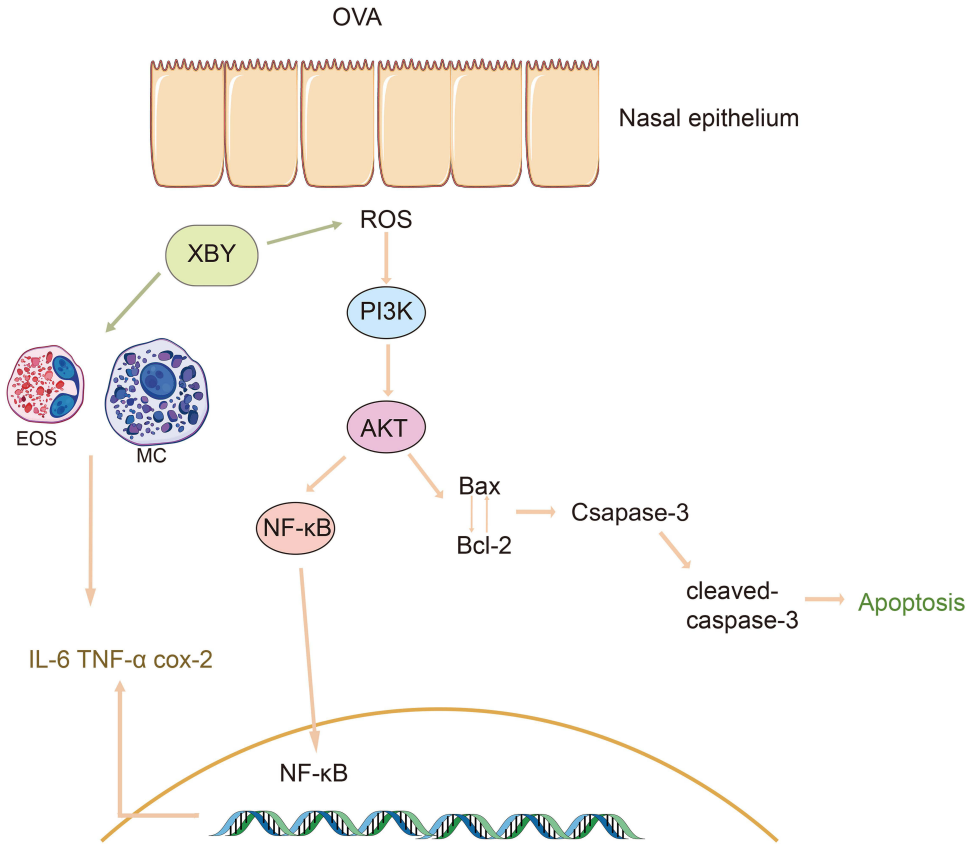

Figure 18 Schematic representation of the signaling pathways mediated by XBY in the treatment of allergic rhinitis.

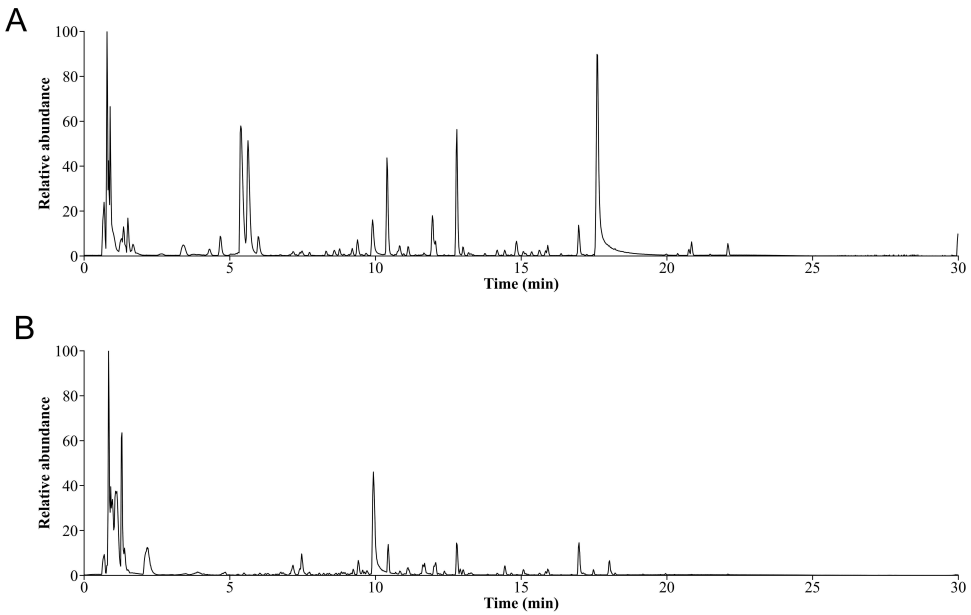

Figure 19 Total ion chromatogram of XBY. (**A**) Positive ion chromatogram; (**B**) negative ion chromatogram.

targeting the PI3K/AKT/NFκB pathway.[38] The pathological findings of this study demonstrate that XBY markedly diminishes EOS and MC infiltration in nasal mucosal tissue, mitigates interstitial edema, and enhances epithelial cell organization; serum concentrations of OVA-sIgE, Total-IgE, IL-6, TNF-α, and COX-2 all exhibit significant reductions; serum levels of ICAM-1 and VCAM-1 were also significantly lowered. The findings suggest that XBY may alleviate the inflammatory milieu of AR, potentially by reducing MC degranulation and inhibiting EOS chemotaxis.

The dynamic imbalance between apoptosis and inflammatory responses is a critical characteristic of the disease process in AR.[39] Bcl-2 and Bax are crucial in regulating apoptosis. Prior research has demonstrated that Bcl-2 and Bax participate in biological processes like the cell cycle, proliferation, and apoptosis, and are regulated across the PI3K/AKT signal transduction pathway.[40] In the context of persistent inflammatory stimulation in AR, ROS levels rise aberrantly, perpetually activating the PI3K/AKT signaling pathway, inhibiting Bax expression, stabilizing Bcl-2, and concurrently inhibiting Caspase-3 cleavage, thus sustaining the pathological survival of inflammatory cells, including EOS and MC. Due to abnormal anti-apoptotic signals, nasal mucosal tissue cells progressively forfeit their typical regenerative and reparative abilities, resulting in compromised nasal mucosal barrier function, enhanced infiltration of inflammatory factors, and establishment of an oxidative stress microenvironment. Based on previous studies, this work suggests that XBY may contribute to inflammation-induced abnormal cell death and tissue damage in AR, potentially through modulation of the PI3K/AKT pathway and alterations in Bcl-2 and Bax levels. The findings of this study indicated that the XBY intervention increased Bax, Cleaved-Caspase-3, and Caspase-3 expression; decreased Bcl-2 expression; and diminished the quantity of apoptotic cells as measured by FCM. These observations imply that XBY could potentially prevent cell death by affecting the PI3K/AKT pathway, restoring the balance between Bcl-2 and Bax, and alleviating the nasal mucosa's inflammatory environment.

The findings suggest that XBY might modulate the ROS/PI3K/AKT/NFκB signaling pathway in treating AR, potentially reducing the release of inflammatory factors, inhibiting apoptosis, alleviating allergic inflammatory responses, and improving the condition of the nasal mucosa (Figure 18). This study employed TCM mass spectrometry technology to analyze the primary active components of the drug in the XBY formulation, as illustrated in Figure 19. The findings indicated that the predominant components were Genkwanin, Calycosin, Kaempferol, and Luteolin, chiefly sourced from *Ephedra herba, Hedysarum multijugum maxim*, and *Cortex moutan*. Prior research has established that Genkwanin, Calycosin, Kaempferol, and Luteolin demonstrate substantial anti-tumor and anti-inflammatory properties. Genkwanin significantly diminishes the expression of inflammatory mediators such as TNF-α, IL-6, and COX-2 while also reducing the phosphorylation levels of Ikk, IκB, and NFκB, thereby inhibiting the NFκB pathway.[41] Calycosin attenuates NFκB activation in allergic conditions, mitigating inflammatory responses,[42] and alleviates chondrocyte inflammation and apoptosis by inhibiting the PI3K/AKT/NFκB pathway.[43] Kaempferol and Luteolin effectively suppress airway reactivity and diminish airway inflammation in managing allergic asthma.[44] The test results may provide some insight into the rationale and potential efficacy of XBY therapy for androgenetic alopecia.

Although this study provides evidence supporting the use of XBY in treating AR, limitations exist, such as a small sample size and a short model duration. Further investigation into the mechanisms and active components of XBY could yield more reliable and precise results, thereby offering a more comprehensive understanding of XBY's therapeutic effects on AR.

Conclusion

The experimental results suggest that XBY treatment for AR might be associated with modulation of the ROS/PI3K/AKT/NFκB signaling pathway. By reducing inflammatory cell infiltration, downregulating the expression of inflammatory and adhesion factors, and modulating apoptosis proteins to accelerate inflammatory cell apoptosis, dual mechanisms effectively suppress the progression of inflammation. This study holds potential translational prospects and may provide new insights for the treatment of AR with TCM.

Abbreviations

AR, allergic rhinitis; IgE, immunoglobulin E; TCM, traditional Chinese medicine; MC, mast cells; EOS, eosinophils; ROS, reactive oxygen species; IL-6, interleukin-6; TNF-α, tumor necrosis factor; COX-2, cyclooxygenase-2; ICAM-1,

intercellular cell adhesion molecule-1; VCAM-1, vascular cell adhesion molecule-1; PI3K, phosphoinositide 3-kinase; AKT, protein kinase B; NFκB, nuclear factor kappa-B; Bcl-2, B-cell lymphoma-2; Bax, Bcl-2-associated X protein; HE, hematoxylin and eosin; WB, Western blot; FCM, flow cytometry; GO, Gene Ontology; KEGG, Kyoto Encyclopedia of Genes and Genomes; OVA-sIgE, OVA-specific IgE; PPI, protein-protein interaction; XBY-L, low-dose Xin'an BiYan; XBY-M, medium-dose XBY; XBY-H, high-dose XBY; CH, cetirizine hydrochloride; CC, Cellular Component; BP, Biological Process; MF, Molecular Function.

Data Sharing Statement

TCMSP Chinese herbal medicine database (https://old.tcmsp-e.com/tcmsp.php/); HERB Chinese herbal medicine database (http://herb.ac.cn/); SMILES numbers were acquired from PubChem (https://pubchem.ncbi.nlm.nih.gov/); The GeneCards database (https://www.genecards.org/); The OMIM database (https://www.omim.org/); The DisGeNet database (https://www.disgenet.org/); The TDD database (https://db.idrblab.net/); The STRING database (https://cn.string-db.org/).

Ethics Approval and Consent to Participate

Animal ethics have been approved by the Animal Ethics Committee of Anhui University of Chinese Medicine. Ethics approval number: AHUCM-mouse-2024020.

Ethics for human life science and medical research have been approved by the Medical Ethics Committee of the First Affiliated Hospital of Anhui University of Chinese Medicine. Ethics approval number: 2024AH-09. All animal procedures in this study were carried out in accordance with the Guide for the Care and Use of Laboratory Animals (NIH Publication No. 5-23, revised 1996; NIH, Bethesda, MD, USA).

Consent to Publish

All authors gave their consent for publication.

Acknowledgments

We extend our sincere gratitude to all staff members and participants of this study for their invaluable contributions.

Author Contributions

All authors made a significant contribution to the work reported, whether that is in the conception, study design, execution, acquisition of data, analysis and interpretation, or in all these areas; took part in drafting, revising or critically reviewing the article; gave final approval of the version to be published; have agreed on the journal to which the article has been submitted; and agree to be accountable for all aspects of the work.

Funding

1. Anhui Province Higher Education Natural Science Research Fund (Major Project, 2024AH040150): Clinical and Mechanistic Study on the Prevention and Treatment of Pediatric Adenoid Hypertrophy Based on Zheng's Laryngology Method of Nourishing Yin and Preserving Essence. 2. Song Ruohui, Anhui Province Famous Traditional Chinese Medicine Practitioner Studio (Anhui Traditional Chinese Medicine Development Secret [2024] No. 19). 3. Anhui Provincial Red Cross Society Traditional Chinese Medicine Inheritance and Innovation Development Project (No. 2022ZYYD09).

Disclosure

All authors declare that there are no conflicts of interest in this work.

References

1. Brożek JL, Bousquet J, Agache I, et al. Allergic rhinitis and its impact on asthma (ARIA) guidelines-2016 revision. *J Allergy Clin Immunol*. 2017;140(4):950–958. doi:10.1016/j.jaci.2017.03.050
2. Bousquet J, Anto JM, Bachert C, et al. Allergic rhinitis. *Nat Rev Dis Primers*. 2020;6(1):95. doi:10.1038/s41572-020-00227-0
3. Zhang Y, Lan F, Zhang L. Update on pathomechanisms and treatments in allergic rhinitis. *Allergy*. 2022;77(11):3309–3319. doi:10.1111/all.15454

4. Platt M. Pharmacotherapy for allergic rhinitis. *Int Forum Allergy Rhinol*. 2014;4 Suppl 2:S35–40. doi:10.1002/alr.21381
5. Oktemer T, Altıntoprak N, Muluk NB, et al. Clinical efficacy of immunotherapy in allergic rhinitis. *Am J Rhinol Allergy*. 2016;30(5):4–7. doi:10.2500/ajra.2016.30.4368
6. Yu J, Zhong N, Luo Q, et al. Early efficacy analysis of cluster and conventional immunotherapy in patients with allergic rhinitis. *Ear Nose Throat J*. 2021;100(5):378–385. doi:10.1177/0145561319863370
7. Fang PD, Chen JH, Chen YL, Yang QT, Zhang YN. Management of adverse reactions in allergen-specific immunotherapy for allergic rhinitis. *Zhonghua Er Bi Yan Hou Tou Jing Wai Ke Za Zhi*. 2024;59(1):78–85. doi:10.3760/cma.j.cn115330-20230929-00121
8. Meltzer EO, Szwarcberg J, Pill MW. Allergic rhinitis, asthma, and rhinosinusitis: diseases of the integrated airway. *J Manag Care Pharm*. 2004;10 (4):310–317. doi:10.18553/jmcp.2004.10.4.310
9. Chu YL, T XH, Yan AH. Pathogenesis and treatment of allergic rhinitis. *J Aerospace Med*. 2020;31(03):350–354.
10. Of Rhinology SG. [Chinese guideline for diagnosis and treatment of allergic rhinitis (2022, revision)]. *Zhonghua Er Bi Yan Hou Tou Jing Wai Ke Za Zhi*. 2022;57(2):106–129. in Chinese, Hawaiian. doi:10.3760/cma.j.cn115330-20211228-00828
11. Sotsios Y, Ward SG. Phosphoinositide 3-kinase: a key biochemical signal for cell migration in response to chemokines. *Immunol Rev*. 2000;177 (1):217–235. doi:10.1034/j.1600-065x.2000.17712.x
12. Wu G, Zhu H, Wu X, et al. Anti-allergic function of α-Tocopherol is mediated by suppression of PI3K-PKB activity in mast cells in mouse model of allergic rhinitis. *Allergol Immunopathol*. 2020;48(4):395–400. doi:10.1016/j.aller.2019.11.005
13. Guo Q, Jin Y, Chen X, et al. NF-κB in biology and targeted therapy: new insights and translational implications. *Signal Transduct Target Ther*. 2024;9(1):53. doi:10.1038/s41392-024-01757-9
14. Qin Z, Wang C, Li Y. Exploration of the correlation between oxidative stress and the pathogenesis of allergic rhinitis and the prevention and treatment strategies of traditional Chinese medicine. *J Liaoning Univ Traditional Chin Med*. 2024;26(05):213–220. in Chinese.
15. Liu J, Han X, Zhang T, Tian K, Li Z, Luo F. Reactive oxygen species (ROS) scavenging biomaterials for anti-inflammatory diseases: from mechanism to therapy. *J Hematol Oncol*. 2023;16(1):116. doi:10.1186/s13045-023-01512-7
16. Moradi S, Khazaei H, Tarlan M, et al. Natural products for the treatment of allergic rhinitis: focus on cellular signaling pathways and pharmacological targets. *Front Pharmacol*. 2024;15:1447097. doi:10.3389/fphar.2024.1447097
17. Li J, Li H, Liu HX. Effects of modified xiaochaihu decoction on TCM symptoms and immune function in allergic rhinitis. *World Chinese Med*. 2023;18(24):3547–3550+3555. in Chinese.
18. Lei CF, Zhai CM, Mang CY, et al. A clinical study on treating allergic rhinitis of yangxu feihan type with the Shuangxin Biqiupowder. *Clin J Chinese Med*. 2020;12(19):11–16. in Chinese.
19. Zhang Y, Qi L, Wang R. Meta-analysis: reducing the recurrence rate of allergic rhinitis through oral administration of traditional Chinese medicine. *Eur Rev Med Pharmacol Sci*. 2023;27(17):7924–7934. doi:10.26355/eurrev_202309_33551
20. Zhao XJ. Experimental models of nasal hypersensitive reaction. *Zhonghua Er Bi Yan Hou Ke Za Zhi*. 1993;28(1):17–8,58–9.
21. Moitra S, Mahesh PA, Moitra S. Allergic rhinitis in India. *Clin Exp Allergy*. 2023;53(7):765–776. doi:10.1111/cea.14295
22. Li S, Wu W, Wang G, et al. Association between exposure to air pollution and risk of allergic rhinitis: a systematic review and meta-analysis. *Environ Res*. 2022;205:112472. doi:10.1016/j.envres.2021.112472
23. Liu T, Zhang R, Jiang L, et al. The potential application and molecular mechanisms of natural products in the treatment of allergic rhinitis: a review. *Phytomedicine*. 2024;129:155663. doi:10.1016/j.phymed.2024.155663
24. Liu C, He Y, Zhou K, et al. Mitigation of allergic asthma in mice: a compound mixture comprising luteolin, arbutin, and marmesin from gerbera piloselloides Herba by suppression of PI3K/Akt pathway. *Heliyon*. 2024;10(19):e37632. doi:10.1016/j.heliyon.2024.e37632
25. Ou X, Chen X, Fang Z, Zhao J. Proanthocyanidin B2 alleviates Pg.LPS-induced RAW264.7 cellular inflammation and oxidative stress via PI3K/Akt/NFkB pathway. *Cytotechnology*. 2025;77(2):77. doi:10.1007/s10616-025-00734-6
26. Jutel M, Agache I, Zemelka-Wiacek M, et al. Nomenclature of allergic diseases and hypersensitivity reactions: adapted to modern needs: an EAACI position paper. *Allergy*. 2023;78(11):2851–2874. doi:10.1111/all.15889
27. Olivier CE, Pinto DG, Teixeira APM, et al. Evaluating non-IgE-mediated allergens' immunoreactivity in patients with "intrinsic" persistent rhinitis with help of the leukocyte adherence inhibition test. *European J Med Health Sci*. 2023;5(1):17–22. doi:10.24018/ejmed.2023.5.1.1624
28. Ponda P, Carr T, Rank MA, Bousquet J. Nonallergic rhinitis, allergic rhinitis, and immunotherapy: advances in the last decade. *J Allergy Clin Immunol Pract*. 2023;11(1):35–42. doi:10.1016/j.jaip.2022.09.010
29. Song Y, Chen Y, Cai H, et al. Lentinan attenuates allergic airway inflammation and epithelial barrier dysfunction in asthma via inhibition of the PI3K/AKT/NF-κB pathway. *Phytomedicine*. 2024;134:155965. doi:10.1016/j.phymed.2024.155965
30. Milkovic L, Cipak Gasparovic A, Cindric M, Mouthuy PA, Zarkovic N. Short overview of ROS as cell function regulators and their implications in therapy concepts. *Cells*. 2019;8(8):793. doi:10.3390/cells8080793
31. Li Y, Xia J, Jiang N, et al. Corin protects H(2)O(2)-induced apoptosis through PI3K/AKT and NF-κB pathway in cardiomyocytes. *Biomed Pharmacother*. 2018;97:594–599. doi:10.1016/j.biopha.2017.10.090
32. Hu S, Zhang Y, Dang B, et al. Myricetin alleviated immunologic contact urticaria and mast cell degranulation via the PI3K/Akt/NF-κB pathway. *Phytother Res*. 2023;37(5):2024–2035. doi:10.1002/ptr.7726
33. Pawankar R, Yamagishi S, Takizawa R, Yagi T. Mast cell-IgE-and mast cell-structural cell interactions in allergic airway disease. *Curr Drug Targets Inflamm Allergy*. 2003;2(4):303–312. doi:10.2174/1568010033484016
34. Eifan AO, Durham SR. Pathogenesis of rhinitis. *Clin Exp Allergy*. 2016;46(9):1139–1151. doi:10.1111/cea.12780
35. Lee KS, Lee HK, Hayflick JS, Lee YC, Puri KD. Inhibition of phosphoinositide 3-kinase delta attenuates allergic airway inflammation and hyperresponsiveness in murine asthma model. *FASEB j*. 2006;20(3):455–465. doi:10.1096/fj.05-5045com
36. Chen T, Zhang X, Zhu G, et al. Quercetin inhibits TNF-α induced HUVECs apoptosis and inflammation via downregulating NF-kB and AP-1 signaling pathway in vitro. *Medicine*. 2020;99(38):e22241. doi:10.1097/md.0000000000022241
37. Kong DH, Kim YK, Kim MR, Jang JH, Lee S. Emerging roles of vascular cell adhesion molecule-1 (VCAM-1) in immunological disorders and cancer. *Int J Mol Sci*. 2018;19(4):1057. doi:10.3390/ijms19041057
38. Ye J, Piao H, Jiang J, et al. Polydatin inhibits mast cell-mediated allergic inflammation by targeting PI3K/Akt, MAPK, NF-κB and Nrf2/HO-1 pathways. *Sci Rep*. 2017;7(1):11895. doi:10.1038/s41598-017-12252-3

39. Zhang Y, Song Y, Wang C, et al. Panax notoginseng saponin R1 attenuates allergic rhinitis through AMPK/Drp1 mediated mitochondrial fission. *Biochem Pharmacol*. 2022;202:115106. doi:10.1016/j.bcp.2022.115106
40. Wang R, Song F, Li S, Wu B, Gu Y, Yuan Y. Salvianolic acid A attenuates CCl(4)-induced liver fibrosis by regulating the PI3K/AKT/mTOR, Bcl-2/Bax and caspase-3/cleaved caspase-3 signaling pathways. *Drug Des Devel Ther*. 2019;13:1889–1900. doi:10.2147/dddt.S194787
41. Sun YW, Bao Y, Yu H, et al. Anti-rheumatoid arthritis effects of flavonoids from Daphne genkwa. *Int Immunopharmacol*. 2020;83:106384. doi:10.1016/j.intimp.2020.106384
42. Tao Y, Wang Y, Wang X, et al. Calycosin suppresses epithelial derived initiative key factors and maintains epithelial barrier in allergic inflammation via TLR4 mediated NF-κB pathway. *Cell Physiol Biochem*. 2017;44(3):1106–1119. doi:10.1159/000485416
43. Shi X, Jie L, Wu P, et al. Calycosin mitigates chondrocyte inflammation and apoptosis by inhibiting the PI3K/AKT and NF-κB pathways. *J Ethnopharmacol*. 2022;297:115536. doi:10.1016/j.jep.2022.115536
44. Qin Z, Chen Y, Liu N, et al. Mechanisms of Bushenyiqi decoction in the treatment of asthma: an investigation based on network pharmacology with experimental validation. *Front Pharmacol*. 2024;15:1361379. doi:10.3389/fphar.2024.1361379